Assessment and inter-comparison of recently developed/reprocessed microwave satellite soil moisture products using ISMN ground-based measurements

A. Al-Yaari, J.-P. Wigneron, W. Dorigo, A. Colliander, T. Pellarin, S. Hahn, Arnaud Mialon, Philippe Richaume, R. Fernandez-Moran, L. Fan, et al.

Assessment and inter-comparison of recently developed/reprocessed microwave satellite soil moisture products using ISMN ground-based measurements

A. Al-Yaari[a], J.-P. Wigneron[a], W. Dorigo[b], A. Colliander[c], T. Pellarin[d], S. Hahn[b], A. Mialon[e], P. Richaume[e], R. Fernandez-Moran[f], L. Fan[a,g], Y. H. Kerr[e], G. De Lannoy[h]

[a]INRA, UMR1391 ISPA, Villenave d'Ornon, France, amen.al-yaari@inra.fr,

[b]Department of Geodesy and Geoinformation, Vienna University of Technology, Vienna, Austria

[c]Jet Propulsion Laboratory, California Institute of Technology, Pasadena CA91109, USA

[d]Univ. Grenoble Alpes, CNRS, IRD, Grenoble INP, IGE, F-38000 Grenoble, France

[e] Université de Toulouse, CNES, CNRS,INRA, IRD, UPS, UMR 5126, Toulouse France

[f]University of Valencia, IPL (Image Processing Laboratory), Spain

[g]Collaborative Innovation Center on Forecast and Evaluation of Meteorological Disaster, School of Geographical Sciences, Nanjing University of Information Science and Technology, Nanjing 210044, China

[h]KULeuven, Department of Earth and Environmental Sciences, Belgium

Abstract

Soil moisture (SM) is a key state variable in understanding the climate system through its control on the land surface energy, water budget partitioning, and the carbon cycle. Monitoring SM at regional scale has become possible thanks to microwave remote sensing. In the past two decades, several satellites were launched carrying on board either radiometer (passive) or radar (active) or both sensors in different frequency bands with various spatial and temporal resolutions. Soil moisture algorithms are in rapid development and their improvements/revisions are ongoing. The latest SM retrieval products and versions of products that have been recently released are not yet, to our knowledge, comprehensively evaluated and inter-compared over different ecoregions and climate conditions. The aim of this paper is to comprehensively evaluate the most recent microwave-based SM retrieval products available from NASA's (National Aeronautics and Space Administration) SMAP (Soil Moisture Active Passive) satellite, ESA's led mission (European Space Agency) SMOS (Soil Moisture and Ocean Salinity) satellite, ASCAT (Advanced Scatterometer) sensor on board the meteorological operational (Metop) platforms Metop-A and Metop-B, and the ESA Climate Change Initiative (CCI) blended long-term SM time series. More specifically, in this study we compared SMAPL3 V4, SMOSL3 V300, SMOSL2 V650, ASCAT H111, and CCI V04.2 and the new SMOS-IC (V105) SM product. This evaluation was achieved using four statistical scores: Pearson correlation (considering both original observations and anomalies), RMSE, unbiased RMSE, and Bias between remotely-sensed SM retrievals and ground-based measurements from more than 1000 stations from 17 monitoring networks, spread over the globe, disseminated through the International Soil Moisture Network (ISMN). The analysis reveals that the performance of the remotely-sensed SM retrievals generally varies depending on ecoregions, land cover types, climate conditions, and between the monitoring networks. It also reveals that temporal sampling of the data, the frequency of data in time and the spatial coverage, affect the performance metrics. Overall, the performance of SMAP and SMOS-IC products compared slightly better with respect to the ISMN *in situ* observations than the other remotely-sensed products.

1. Introduction

Surface soil moisture (i.e. the water content in the first few centimeters of the soil; referred to as SM in the following) is a key state variable in better understanding the climate system through controlling land surface energy, water budget partitioning (Chen et al., 2016; Koster et al., 2004; Miralles et al., 2014a; Miralles et al., 2014b; Pitman, 2003; Seneviratne et al., 2010; Seneviratne et al., 2013), and its important role in the carbon cycle (Jung et al., 2017). Monitoring SM at the regional scale has become possible thanks to active and passive microwave remote sensing. In the past two decades, several satellites were launched carrying either a radiometer (passive) or radar (active) or both, using frequency bands with various spatial and temporal resolutions. These satellites (or sensors) include, but are not limited to, SMAP (Soil Moisture Active Passive) launched by the National Aeronautics and Space Administration (NASA) in 2015 (Entekhabi et al., 2010), SMOS (Soil Moisture and Ocean Salinity) launched by the European space agency (ESA) in 2009 (Kerr et al., 2001), and ASCAT (Advanced Scatterometer) (Wagner et al., 2013) on board the meteorological operational (Metop) platforms Metop-A, Metop-B, and Metop-C. Since then, SM was retrieved from either brightness temperature (passive) or backscatter coefficient (active) observations relying mainly on radiative transfer model inversion (passive; Mo et al., 1982), change detection (active; Wagner et al., 1999), or neural network algorithms (Kolassa et al., 2018; Rodríguez-Fernández et al., 2016). These remotely sensed SM products are provided separately or blended (such as the one produced by the ESA project: Climate Change Initiative (CCI) SM long time series (Dorigo et al., 2017; Liu et al., 2012)).

Performance evaluation of these remotely-sensed SM retrievals is important to help improving satellite products and evaluating their interest for possible applications in climate, hydrology, and natural hazards (flood, drought, etc.). Numerous validation/evaluation studies of satellite-based SM retrievals have been conducted during the last decade (e.g., Al-Yaari et al.,

2014a; Al-Yaari et al., 2014b; Al-Yaari et al., 2015; Al-Yaari et al., 2017; Albergel et al., 2009; Albergel et al., 2012; Brocca et al., 2011; Colliander et al., 2017; Dorigo et al., 2015; Draper et al., 2009; Kerr et al., 2016; Pierdicca et al., 2013; Sahoo et al., 2008; Su et al., 2013) using different approaches (e.g., sparse and dense networks, core validation sites, field campaigns, inter-comparisons among satellites, model simulations, etc.). However, SM retrieval algorithms are in rapid development and their improvements/revisions are ongoing adopting new concepts or conducting new calibrations; thus improving parameterizations and optimizing parameters in the algorithms (Wigneron et al., 2017). Therefore, new SM products and new versions of SM products have been released that are not, to our knowledge, comprehensively evaluated and inter-compared yet. One such new product is the SMOS-IC SM product, which was recently developed by INRA (Institut National de la Recherche Agronomique) in collaboration with CESBIO (Centre d'Etudes Spatiales de la BIOsphere) (Fernandez-Moran et al., 2017b). To our knowledge, the last SMOS-IC version has only been evaluated against modelled SM data from ECMWF (Fernandez-Moran et al., 2017b), although a previous version was already tested using several *in situ* datasets from ISMN (International Soil Moisture Network) for the period 2011-2013 (Fernandez-Moran et al., 2017a). The objective of this study is to evaluate the SMOS-IC SM product along with the most recent versions, available at the time of writing, of five other satellite-based SM products, namely: NASA SMAP Level 3 (V4), ESA SMOS Level 3 (V300) and Level 2 (V650), ASCAT (H111), and the CCI long-term record SM (V04.2). This was achieved using ground-based surface SM measurements from the ISMN (Dorigo et al., 2011; Dorigo et al., 2013). For the passive sensors, we limited this study to L-band SM retrievals which are more optimal for monitoring SM. Other key SM observations (AMSR-E/AMSR2) were merged in the CCI product. This paper is organized as follows. The datasets and scores used are briefly described in Section 2. Results and discussion are presented in Sections 3 and 4, respectively. Finally, concluding remarks are given in Section 5.

2. Materials and Methods

2.1 Datasets

Table 1 presents an overview of the SM products used in this study. More details are given in the following subsections.

Table 1. Overview of all soil moisture data sets under investigation.

	Passive		**Active**	**Combined (CCI)**
Sensor	SMOS	SMAP	ASCAT	SMMR SSM/I TMI AMSRE AMSR2 Windsat ERS ASCAT SMOS
Satellite	SMOS	SMAP	Metop-A & Metop-B	Various
Time period	Jan 2010–present	Mar 2015–present	Jan 2007–present	Jan 1978–Dec 2016
Band frequency	1.4 GHz	1.4 GHz	5.3 GHz	1.4–19.3 GHz
Spatial sampling	15 km DGG - 25 km EASEv2	36 km EASEv2	12.5 km	0.25°
Sensor resolution	27-55 km	43 km	25-34 km	various
Spatial coverage	Global	Global	Global	Global
Acquisition time	Descending: 06:00 pm Ascending: 06:00 am	Descending: 06:00 am Ascending: 06:00 pm	Descending: 09:30 am Ascending 9:30 pm	-
Product version	SMOSL2 V650 SMOSL3 V300 SMOS-IC V105	SMAPL3 V4	H111	CCI V04.2
Unit	m^3/m^3	m^3/m^3	Degree of saturation (%)	m^3/m^3

2.1.1 SMOS

The SMOS satellite, developed by the ESA with contributions from CNES (Centre National d'Etudes Spatiales) and CDTI (Centro para el Desarrollo Tecnológico Industrial), is the first polar orbiting L-Band (1.4 GHz) radiometer, with a spatial resolution of (~ 43 km) and 3-day revisit. The SMOS satellite mission has been providing fully polarized brightness temperature (TB, level 1) observations since 2010 and over a range of incidence angles (~ 0-

60°) (Kerr et al., 2010). These SMOS TB observations are used to retrieve SM and vegetation optical depth (VOD) using a forward emission model, namely, the L-band Microwave Emission of the Biosphere (L-MEB) model (Wigneron et al., 2007). The retrieval approach is simply based on iterative estimation of SM and VOD values providing the lowest difference between modelled and observed TB data by minimizing a cost function (sum of the squared weighted differences between modelled and observed TB) (Wigneron et al., 2000).

Currently, there are three main physically-based SMOS SM retrieval products available (SMOS-IC, SMOS Level 2 (L2), and SMOS Level 3 (L3)), for which all: (i) use the L-MEB radiative transfer model (ii) provide SM as volumetric water content (m^3/m^3) with global coverage of 3 days; (iv) provide data at both ascending (06:00 am) and descending (06:00 pm) orbits; (vi) adopt the NETCDF format for the products; and (vii) use the European Centre for Medium-Range Weather Forecasts (ECMWF) soil temperature products. However, the products differ by the projection and grid used as well as with the temporal aggregation for L3 products sampling, as detailed below. It should be noted that SMOS provides also root zone SM at 0-1 m as Level 4.

2.1.1.1 SMOS-IC

In this study, we used the SMOS-IC V105 SM product. The SMOS-IC SM product is based on a relatively simple approach that considers homogeneous pixels (unlike SMOSL3 and SMOSL2 where the details of the SMOS footprint at a resolution of 4 km x 4 km are taken into account), to avoid possible uncertainties and errors associated with the datasets used to characterize the heterogeneity of the pixel in the SMOSL2 and SMOSL3 algorithms. The SMOS-IC inversion algorithm aims at a minimal use of auxiliary data through the optimal use of the multi-angular TB observations. Therefore, SMOS-IC (unlike SMOSL2 and SMOSL3) does not use ECMWF SM or the Moderate Resolution Imaging Spectroradiometer (MODIS) LAI (Leaf Area Index) products as first guesses and in the simulation of TB over

heterogeneous pixels including forested areas. In SMOS-IC, the effective vegetation scattering albedo (ω) parameter was optimized using the ISMN in-situ observations (Fernandez-Moran et al., 2017a) and the roughness parameters were derived from the global map of Parrens et al. (2016). The "optimization" process of ω led to a very simple result: ω ~ 0.1 over low vegetation and bare soils, while ω ~ 0.06 over forested areas. Also, SMOS-IC does not take into account the corrections associated with the characterization of the antenna patterns as a function of viewing angle and azimuth. To filter out observations/retrievals strongly impacted by RFI (the probability of instantaneous radio frequency interferences) effects, SMOS-IC SM retrievals were excluded when the Root Mean Square Error (RMSE) between SMOSL3 TB and simulated TB > 10 K in the present study. SMOS-IC is currently delivered as a scientific product in the Equal-Area Scalable Earth (EASE) grid version 2 at 25 km resolution and publicly available at CATDS (Centre Aval de Traitement des Données SMOS): https://www.catds.fr/Products/Available-products-from-CEC-SM/SMOS-IC. Note that although SMOS-IC was recently released, it corresponds to the initial SMOS 2-Parameter retrieval approach, relying on the relatively low temporal variation of VOD, and fully described in Wigneron et al. (2000). Also note that SMOS-IC is currently in its first version and is thus prone to evolve and progress as it is still undergoing refinements and improvements.

2.1.1.2 SMOSL2

In this study, we used the SMOSL2 SM product in version V650. There are some changes in this version relative to the previous ones (e.g., V620) such as updating some processing parameters (e.g., Chi^2 rescaling), configuration (that can be used for additional quality control checks), and auxiliary files. The most important one is replacing the ECOCLIMAP (218 ecosystems) database (Masson et al., 2003) with the International Geosphere Biosphere Programme (IGBP; 17 land cover classes) land cover map (Friedl et al., 2010), which is

also used by the SMAP Level 2 algorithm. This change influences the distribution of the forested areas (FO) and the nominal vegetated soil and therefore leads to different SM values from previous versions.

SMOSL2 (and SMOSL3) algorithm considers pixel heterogeneity and inversion is done on the dominant fraction: low vegetation, bare soil or forest and water surfaces. On the non-dominant fraction, auxiliary information (e.g., ECMWF SM and MODIS LAI_{Fmax}, the maximum yearly value of LAI) is used to simulate TB and to better constrain the model inversion. However, these auxiliary data contain errors that can propagate in the inversion algorithm, which may lead to noise and bias in the SM retrievals. In the latest SMOSL2 version, ECMWF SM is used to simulate TB over heterogeneous pixels including forested areas after re-scaling. This was done by using cumulative distribution function (CDF) matching, to better match to the histogram of the SMOS SM retrieved values.

SMOSL2 SM is provided in swath mode in the Icosahedral Equal Area (ISEA) 4H9 Discrete Global Grid (DGG) at 15 km resolution and can be freely obtained from the ESA website portal https://earth.esa.int/web/guest/missions/esa-operational-eo-missions/smos. Readers are referred to Kerr et al. (2012) for more details. SMOSL2 SM retrievals were filtered excluding the following: Chi^2 index (i.e. retrieval fit quality index between the observed SMOS TBs and the simulated TBs) > 3 and RFI > 20%; where RFI was calculated as follows:

$$RFI = \frac{NRFI_x + NRFI_y}{MAVA0} \quad (1)$$

where:

NRFIx: is the number of TB flagged for RFI in the X–direction.

NRFIy: is the number of TB flagged for RFI in the Y–direction.

MAVA0: is the total number of TB observations at this point.

2.1.1.3 SMOSL3

202 The SMOSL3 SM algorithm is based on the same complex approach (i.e. accounting
203 for heterogeneity) used in the SMOSL2 but enhanced through a multi-orbit algorithm that
204 uses retrievals from several revisits over a seven day window (Al Bitar et al., 2017; Jacquette et al.,
205 2013). In addition, the objective of SMOSL3 is to provide enhanced products that are easier to
206 process by the scientific community, given as daily, aggregated in 3-days (moving window
207 mean), 10-days (median, minimum and maximum values), and monthly (mean) global maps.
208 Here we used the daily SMOSL3 version 300, which can be freely obtained from the CATDS
209 website portal in the EASE grid v2 (25 km), which is much easier to process than the grid
210 used in the SMOSL2 processor. SMOSL3 SM retrievals were excluded when RFI > 20%.
211 Readers are referred to Al-Bitar et al. (2017) for more details about SMOSL3.
212 It should be noted here that the soil roughness and effective vegetation scattering
213 albedo parameters used in SMOSL2 and SMOSL3 are still pre-launch values and thus
214 different from those currently used in the SMOS-IC algorithm (note that tests made using the
215 SMOS-IC parameters in SMOSL2 did lead in improvements in the L2 SM retrievals). Also
216 note that SMOSL3 is based upon an older version of L2 and that a bug was identified in the
217 current SMOSL3 algorithm (V300) and will be corrected in the next version.

218 **2.1.2 SMAP**

219 SMAP is a NASA satellite mission that was launched in 2015 to monitor global SM
220 and landscape freeze/thaw state (Entekhabi et al., 2010). The SMAP satellite carries a
221 radiometer (operational; 1.41 GHz) and radar (stopped working after about three months of
222 operation; 1.26 GHz) operating in the L-band frequency. The spatial resolution of radar and
223 radiometer is ~ 3 km and ~40 km, respectively, with a 1000-km swath width and a constant
224 40-degree incidence angle. The SMAP mission provides surface (~ 5 cm) SM (Chan et al., 2016)
225 and root zone SM (1 m; Reichle et al., 2017); and also other geophysical variables such as
226 landscape freeze/thaw (Derksen et al., 2017) and net ecosystem exchange of carbon (NEE) (Jones et

al., 2017). Like SMOS, different levels of SM products are delivered as half-orbit products (swath based product; SMAPL2), daily gridded composites (SMAPL3), and model-assimilated products i.e. SMAPL4. In this study, we used the 36-km EASEv2 gridded L3SMP. V4 SM product (only when the retrieval quality is recommended i.e. unfrozen soils and a vegetation water content < 5 kg/m^2). This version (herein referred to as SMAP) was preceded by a beta quality version (released in 2015) and Version 3 validated SM data (released in 2016) (O' Neill et al., 2017).

2.1.3 ASCAT

The Advanced Scatterometer (ASCAT) is a real aperture radar carried on-board Metop-A satellite that was launched in October 2006, followed by Metop-B satellite launched in September 2012 (PUM, 2016). Both satellites share the same sun-synchronous near-polar orbit and are half an orbital period apart from each other (~50 min.). The mean local solar time of the descending node is 9:30 a.m. and 9:30 p.m. for the ascending node. ASCAT operates in the C-band frequency (VV polarization) and measures the Normalized Radar Cross Section (NRCS), also known as backscatter coefficient. The two main ASCAT level 1b backscatter products are provided at a spatial resolution of 25-34 km and 50 km. The Vienna University of Technology (TU Wien) semi-empirical change detection algorithm exploits the multi-angle backscatter measurements from ASCAT in order to obtain surface SM expressed in degree of saturation (Wagner et al., 1999).

In this study, we used Metop ASCAT Surface SM Climate Data Record (CDR) time series obtained from the Satellite Application Facility on Support to Operational Hydrology and Water Management (H SAF), namely, H111 - Metop ASCAT SSM CDR2016: Metop ASCAT SM CDR2016 time series with 12.5 km spatial sampling. Soil moisture values were only kept when the confidence flag [frozen or snow cover probability > 50% and using the Surface State Flag (SSF) information] = 0 (Paulik et al., 2014). The relative surface SM given

254 in degree of saturation was converted into absolute SM (expressed in m^3/m^3) using porosity
255 information (provided with the ASCAT datasets) computed from the Harmonized World Soil
256 Database (HWSD; (FAO et al., 2012)) using the formulas of Saxton and Rawls. (2006). It should
257 be noted that, root zone SM index is produced based on ASCAT SM assimilation in the
258 ECMWF Land Data Assimilation System, namely the H-SAF SM-DAS-2 product. The
259 reader is referred to the Product User Manual (PUM) for more details (PUM, 2016) about
260 ASCAT SM.
261
262 **2.1.4 ESA CCI Soil Moisture**
263 The ESA CCI combined SM product is produced by merging both passive and active
264 SM products (Liu et al., 2012) and available over 11/1978 – 12/ 2016 on global scale. These
265 include scatterometer-based SM data (ERS ½, Metop A/B ASCAT) and radiometer-based
266 SM data (SMMR, SSM/I, TMI, AMSR-E, WindSat, AMSR2, and SMOS). The merging
267 between active and passive SM products is done based on a weighted average method with
268 the weights being proportional to Signal to Noise Ratio (SNR; estimated using triple
269 collocation analysis) of each product (Dorigo et al., 2017; Gruber et al., 2017). It should be noted that
270 all these different datasets are scaled to a common model SM climatology, provided by the
271 Global Land Data Assimilation System (GLDAS) Noah Land Surface Model (Rodell et al., 2004)
272 using a CDF matching technique. Therefore, this study will show the Bias values but will not
273 discuss them as they reflect the GLDAS model.
274 Regions of frozen soils or snow covered soils were already masked in the product
275 obtained from the level 2 quality flags and no data are provided over rainforest regions
276 (Dorigo et al., 2017). More details about the theoretical and algorithmic base of this product
277 and detailed analysis about the uncertainties of the SM datasets can be found in (Dorigo et al.,
278 2017; Gruber et al., 2017; Liu et al., 2012). The reader is also referred to http://www.esa-soilmoisture-

cci.org for more information about the daily CCI volumetric (m^3/m^3) SM product, which is provided in a NETCDF format with a spatial resolution of 0.25° x 0.25° (WGS 84); and can be freely downloaded after registration on the CCI SM Website.

2.1.5 ISMN *in situ* data

The International Soil Moisture Network (ISMN) was initiated in 2009 in order to support the calibration/validation (cal/val) activities of remotely-sensed SM retrievals (Dorigo et al., 2011; Dorigo et al., 2013). More specifically, it was supported by ESA in the framework of the SMOS mission to help in the cal/val activities. Once *in situ* SM observations are collected from international networks, they are quality controlled and harmonized to be distributed through the ISMN website portal: https://ismn.geo.tuwien.ac.at/. Currently, the ISMN database hosts ground-based SM measurements from about ~ 58 networks located all over the world. Some of these datasets (e.g., SCAN, the US Climate Reference Network) are provided in near-real time. The *in situ* SM networks used in this study during the 2010-2017 period are listed in Table S1 and displayed in Fig. S1, covering a variety of climate and vegetation conditions (see supplementary materials) but not all ecosystems are equally well represented. In this study, only SM observations flagged as "Good" were considered in the evaluations (Dorigo et al., 2013). In addition, OZNET and AMMA networks datasets were obtained from http://www.oznet.org.au/mdbdata/mdbdata.html and T. Pellarin (personal communication), respectively. Some networks have their stations distributed over an area that is smaller than the typical footprint of the space borne instruments considered in this study. This results in samples that are not independent in the comparisons, but this was not considered as a problem because the effect is largely the same for each product.

2.2 Methodology

The satellite SM products were evaluated against ground-based measurements following two approaches i) using all available SM retrievals for each product within the period 2010-2017; ii) using common dates (i.e. days where all satellite-based SM observations are available) between the different datasets, either with or without including SMAP. Approach (i) is used assuming that the final users of SM products may use these products separately, and hence limiting the evaluation to common dates may not correspond to the actual accuracy which will be obtained by the end user. SMAP is available for a shorter period compared to the other products, and was therefore either included or excluded in approach (ii) to evaluate the influence of time series length and data sampling in the evaluation. All products used in this study were provided in "a daily time step", therefor, in all these cases the instantaneous overpass times, for each day, were matched with instantaneous in situ measurements within a time window of 1 hour. Dates with no match with in situ observations were not considered in the analyses. In addition, stations with a number of data pairs lower than one month (~31) were excluded from the analyses (e.g., Kolassa et al., 2018). Finally, stations where all remotely-sensed SM products obtained Pearson correlation values (R) lower than 0.5 were screened out.

Four scores, widely used by the SM community, were used here to evaluate the remotely-sensed SM products: Pearson correlation coefficient (R; Eq. 2) to evaluate the ability of satellite-based retrievals on capturing SM seasonal variations of *in situ* measurements, Bias (Eq. 3) to measure the dryness or wetness of the satellite-based retrievals compared to *in situ* observations, RMSE (Root mean square error; Eq. 4), and the unbiased RMSE (ubRMSE; Eq. 5) given as follows:

$$R = \sqrt{1 - \frac{(SM_{RS} - SM_{REF})^2}{\left(SM_{RS} - \overline{SM_{REF}}\right)}} \quad (2)$$

$$Bias = \overline{(SM_{RS} - SM_{REF})} \quad (3)$$

$$RMSE = \sqrt{\overline{(SM_{RS} - SM_{REF})^2}} \quad (4)$$

$$ubRMSE = \sqrt{RMSE^2 - Bias^2} \quad (5)$$

where SM_{RS} is the satellite-based SM, SM_{REF} is the ISMN *in situ* SM used as a reference, and the temporal mean of the entire time series is indicated by an overbar.

The ground-based measurements are based on in situ observations at single location. Therefore, the in situ data have a spatial support that differs largely from the gridded SM retrieval products, which themselves are derived from elliptical footprints. The problem is all the more complex for SMOS, as (i) SMOS retrievals are based on multi-angular observations, and (ii) the available range of the SMOS observations over a given pixel changes from one date to the other (with a sub-cycle of about 16 days). Consequently, all metrics will be prone to representativeness error (Gruber et al., in review). These errors have been earlier analyzed, for example, by Crow et al. (2012) and Famiglietti et al. (2008). These studies showed that the representativeness errors significantly affect the reliability of the metrics in the absolute sense. However, the analysis presented here is comparative in nature and while the representativeness errors also degrade the ability of the comparisons to detect differences between the products, the results carry information on relative merits of the products. Alternative approaches that may mitigate this problem for sparse networks include deployment of triple collocation technique (for example, (Chen et al., 2017a)), but this is outside of the scope of this study. Moreover, the sampling depth can be different among satellites and among in situ sensors thus leading to mismatch in soil depth, which can potentially affect the

evaluation. OZNET network, for instance, measures SM within the 0-5 cm topsoil layer, while most of the other networks measure SM at 5 cm.

Furthermore, the SM seasonal cycle was removed by computing R using anomalies (R_{anom}). This is to evaluate the ability of satellite-based SM retrievals on capturing the day to day variability (short variations) of *in situ* SM observations, which is more important than absolute values for many applications (e.g. data assimilation) and which also reduces part of the representativeness issue mentioned above. The anomaly was computed using the following formula (e.g., Parrens et al., 2012; Rodríguez-Fernández et al., 2016):

$$SM_{anom} = \frac{SM_i - \overline{SM\ (w)}}{SD\ (SM\ (w))} \qquad (6)$$

where SM_i is the SM value at day (i) and $\overline{\mathrm{SM\ (w)}}$ and $\mathrm{SD\ \big(SM\ (w)\big)}$ are the mean and standard deviation over a sliding window (w) of 35 days (Albergel et al., 2012; Brocca et al., 2011), respectively. Note that the seasonalities are not averaged across years into a climatology.

SM time series were extracted from the original grids (e.g., 36 km for SMAP, 25 km for SMOSL3, etc.) from those pixels that correspond to each station separately (based on its latitude and longitude). This being said, it is likely that some stations from a dense network (e.g., OZNET) may correspond to the same passive (SMAP, SMOS, and CCI) pixel but for several active (ASCAT) pixels. Then, the metrics between satellite data and the *in situ* observations were computed separately for each station. Finally, the median of each metric for all stations within a continent was calculated. In addition, the median of each metric for all stations within a land cover type (derived from MODIS (Friedl et al., 2010)), LAI category, or Köppen-Geiger climate zone (Rubel et al., 2017), displayed in Fig. S1 (in the supplementary), was also computed and presented in the following section. Correlation coefficients (R) are

not additive measures and thus cannot be simply averaged; therefore, the median was instead computed. The spatial standard deviation is added to the median skill metrics.

3. Results

3.1 Using all available observations

The four scores (R, Bias, RMSE, and ubRMSE) were computed between remotely-sensed SM retrievals (if available) and 17 ISMN *in situ* observation networks listed in Table S1 in the supplementary. As mentioned before, all observations available within the 2010-2017 period were considered. This being said, the period used to compute the scores for each product can be different.

Fig. 1 shows the overall performance (R, R_{anom}, Bias, RMSE, and ubRMSE scores) of each product stratified by continent. For stations located in Africa, ASCAT had overall slightly higher correlation values but also higher Bias, RMSE, and ubRMSE values than all other SM products. Nonetheless, there are small differences in terms of R between the remotely-sensed SM products (R ranging from ~0.75 to ~0.80). Therefore, temporal SM variations from *in situ* stations over sites in this continent are well reproduced by the remotely-sensed SM products. However, R_{anom} dropped for all the remotely-sensed SM products with higher and similar performances by SMAP and SMOS-IC. Over this region, all products were wetter than the *in situ* observations (consistent with Al-Bitar et al. (2017) for SMOS V300 and Rodríguez-Fernández et al. (2016) for ESA CCI V2.02 SM).

For the U.S. networks (e.g., SCAN, SNOTEL, SOILSCAPE, USCRN, etc.), SMAP had the highest correlation (followed by SMOS-IC), lowest ubRMSE and RMSE values (followed by CCI). In terms of R_{anom}, SMOS-IC had the highest value, whereas the other five

products had similar performances. All data sets were drier than the ISMN observations with the highest Bias values obtained by SMOS-IC.

For the Australian network (OZNET), while SMOS-IC and CCI had the lowest ubRMSE (followed by SMOSL2 SM) and RMSE values, SMAP and SMOS-IC had the highest correlation (original and anomalies) values along with SMOSL2 and SMOSL3. All products were wetter than the *in situ* observations. The results over the OZNET network are consistent with Colliander et al. (2017) who also showed, for instance, that SMAP is wet (although the study was based only on data of the Yanco site and used SMAPL2 V2).

In case of the European networks (e.g., REMEDHUS, SMOSMANIA, BIEBRZA_S-1, RSMN, HOBE, etc.), ESA CCI SM had the lowest overall ubRMSE (followed by SMAP) and RMSE values, while SMAP and SMOS-IC showed the highest values in terms of correlations. SMOS-IC, again, had the highest R_{anom} values. There is a strong variability in terms of Bias for the different products: from an underestimation by all SMOS products to an overestimation by SMAP, ASCAT and the ESA CCI SM.

Generally, the best performance of all remotely-sensed SM products was found over Australian and African stations, while the worst and diverse results were found over the U.S. and Europe. Remarkably, a systematic overestimation or underestimation of the ISMN *in situ* observations has been observed by remotely-sensed SM products over stations located over Africa (and Australia) and America, respectively. Generally, for areas without or with very few RFI (Australia and Africa) SMOS had positive biases but when there are many (Europe) it is always negative (Bircher et al., 2012). It should be noted that some areas are much better represented than others (US vs Africa for instance) in terms of number of points and that for Africa only one ecosystem is considered when it ranges from temperate to arid via tropical.

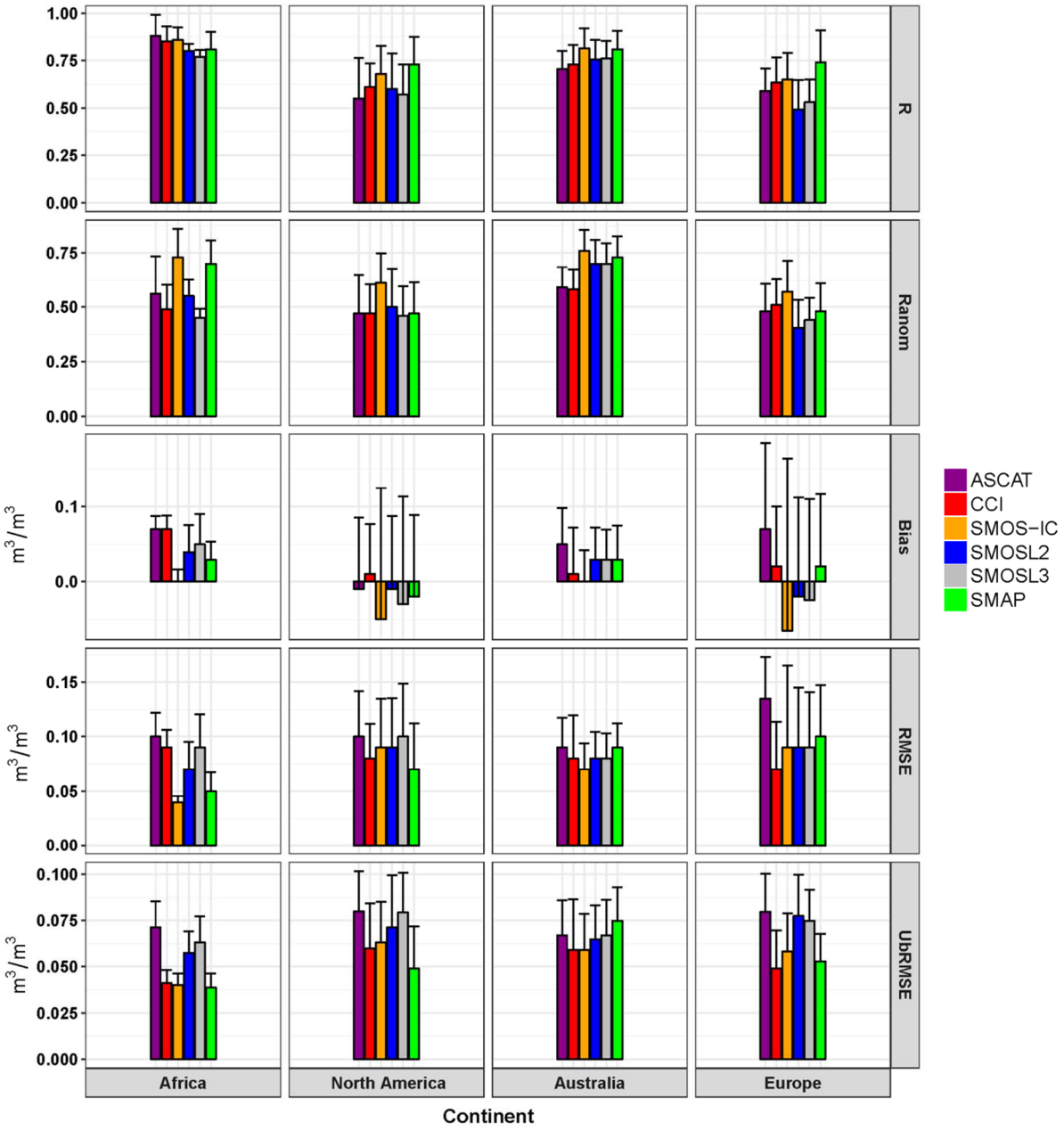

Figure 1 Median evaluation metric (R, R_{anom}, Bias, RMSE, and ubRMSE) for the entire period 2010-2017, across all sites for all products (without data cross masking) compared to ISMN in situ SM, stratified by continent: America (n=448 stations), Australia (n=46 stations), Europe (n=128 stations), and Africa (n=13 stations). Error bars represent the standard deviation (SD; variability) of the station metrics (median+SD) and do not represent anything on the temporal sampling frequency.

3.2 Using only temporally collocated data

3.2.1 For the SMAP period (Jan 2015-Dec 2016)

Here, we limited the analyses to only common dates by doing a temporal collocation between the different satellite-based SM retrievals (Fig. 2). Due to the short period of SMAP,

435 only 9 networks out of 17 were retained: OZNET, PBO_H2o, REMEDHUS, RSMN, SCAN,
436 SMOSMANIA, SNOTEL, SOILSCAPE, and USCRN. As expected, the rank of the product
437 performances in Fig. 2 is different to the one shown in Fig. 1 (without temporal collocation).
438 Over the U.S. networks (North America), SMOS-IC, SMOSL2, and SMAP (ASCAT)
439 had the highest (lowest) correlations (both original and anomalies). There is almost similar
440 performance in terms of R and RMSE values between SMOSL2, SMOS-IC and SMAP but
441 lowest (highest) ubRMSE was obtained by SMAP (SMOSL3 and ASCAT). All products
442 (except for ESA CCI SM, whose bias is the model bias of GLDAS Noah) are drier than the *in*
443 *situ* observations; with, again, marked underestimation by SMOS-IC as already seen in Fig.
444 1. Lower R_{anom} values were obtained by all products but the performance rank of the products
445 was unchanged.
446 Over the Australian network (OZNET), all SMOS versions and SMAP had almost
447 similar performance in capturing the temporal dynamics (both annual cycle and day to day
448 variations) of the ISMN *in situ* observations and better compared to *in situ* observations than
449 ESA CCI SM and ASCAT SM products. SMOS-IC and SMOSL3 (SMAP) had the lowest
450 (highest) ubRMSE values. All SMOS products had similar RMSE values and lower than the
451 other products. All remotely-sensed SM products were wetter than the *in situ* measurements
452 (with the exception of SMOS-IC).
453
454

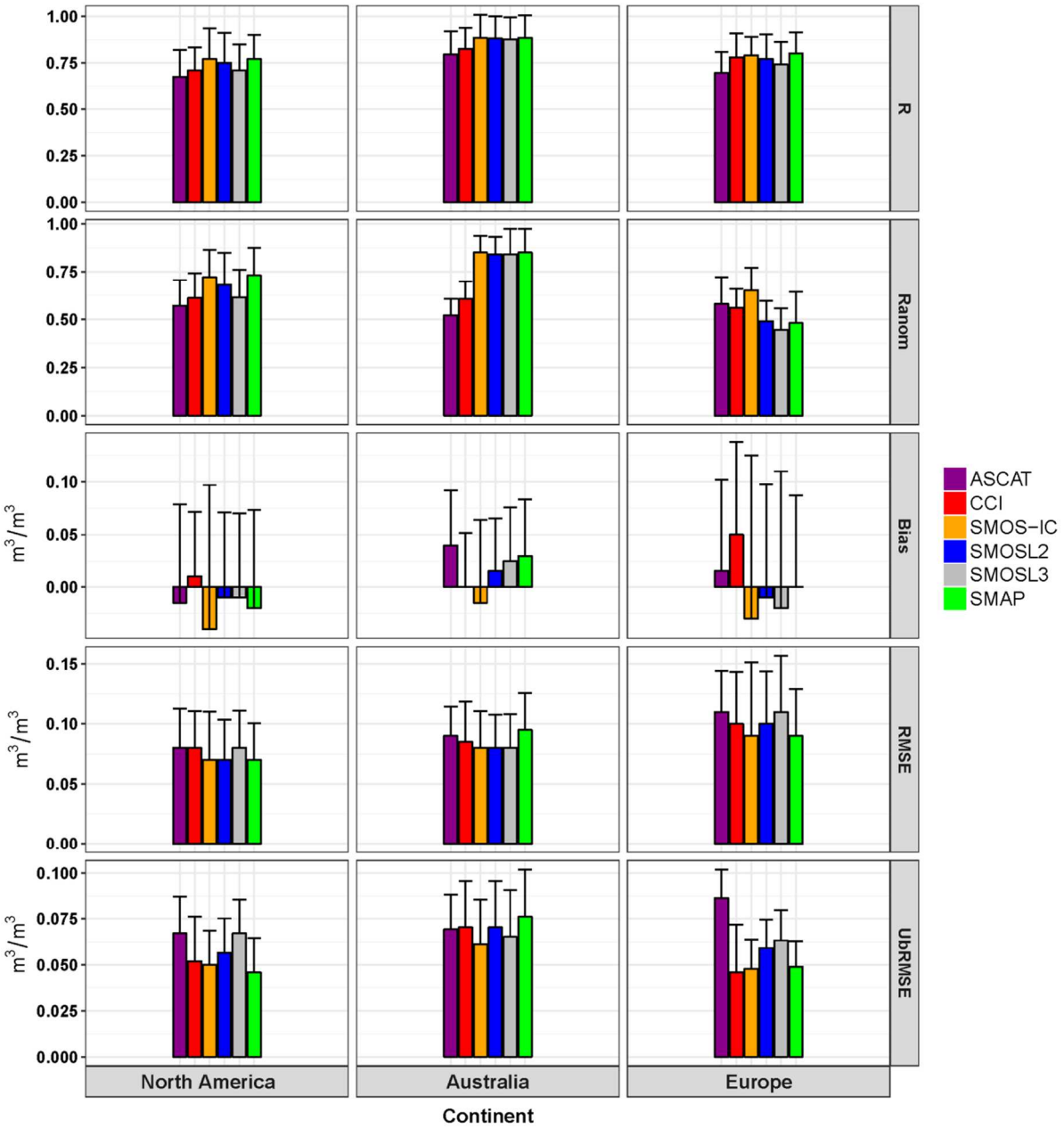

Figure 2 Same as Figure 1, but now only including common data points for each product within the 2015-2016 period, and hence using a reduced number of stations (n) over America (n=174 stations), Australia (n=30 stations), and Europe (n=27 stations).

In case of Europe, there is generally no big difference in terms of correlations between the products but strong differences can be noted in terms of UbRMSE and Bias. SMOS-IC and ASCAT had the highest R_{anom} values against the ISMN observations. Similarly to what was already found in Fig. 1, while all SMOS SM products were drier than the *in situ* measurements, ESA CCI SM and ASCAT were wetter than the *in situ* measurements.

3.2.2 For the period without SMAP (Jan 2010-Dec 2016)

Excluding SMAP, only SMOS, ESA CCI, and ASCAT SM products were considered. Here, fourteen *in situ* SM networks were retained: AMMA, ARM, BIEBRZA_S-1, DAHRA, HOBE, OZNET, PBO_H2O, REMEDHUS, RSMN, SCAN, SMOSMANIA, SNOTEL, SOILSCAPE, and USCRN. As done in Figs. 1 and 2, Fig. 3 shows the overall performance of the remote-sensing SM products stratified per continent.

In the case of sites located over Africa, there are generally strong correlations between satellite-based SM products and the *in situ* observations with similar performances in terms of correlations (R) - with the exception of SMOSL3- and lowest ubRMSE values were obtained by SMOS-IC and ESA CCI SM products. As over America and Europe, no change in terms of Bias from Fig. 1 was found. It should be noted that SMOSL2 outperformed SMOSL3 in most scores, which is in line with the findings of Al Bitar et al. (2017), using SMOSL2 V620 and SMOSL3 V300.

For the U.S. networks, SMOS-IC (followed by SMOSL2 and ESA CCI) presented slightly higher correlation values. SMOS-IC and SMOSL2 presented higher R_{anom} and the other three products performed similarly. As found in Fig. 1, all data were drier than the *in situ* observations except ESA CCI SM which is wetter, with again marked underestimation by

SMOS-IC. Similar and lower RMSE values were obtained by ESA CCI, SMOSL2, and SMOS-IC. Similar and lower ubRMSE values were obtained by ESA CCI and SMOS-IC.

Over the Australian network, the highest correlation values (R and R_{anom}) were obtained by SMOS-IC, SMOSL2, and SMOSL3. The lowest ubRMSE value was obtained by SMOSL2. In general, over Australia, the SMOS SM products perform better than the ESA CCI SM and ASCAT (in line with the findings of Holgate et al. (2016)) products but there are small (or no) differences between the SMOS products and the ESA CCI SM products in terms of RMSE and ubRMSE values with SMOSL2 product being the best for UbRMSE and SMOS-IC for RMSE. No change in terms of sign of Bias from Fig. 1 (although the magnitudes are different).

In the case of sites located over Europe, SMOS-IC (followed by ESA CCI SM and ASCAT), again performed slightly better in terms of correlations (R and R_{anom}) than the other products but the lowest ubRMSE values were obtained by ESA CCI SM. Lowest RMSE values were obtained by ESA CCI, SMOSL3, and SMOSL2. No change in terms of sign of Bias can be noted in comparison to Fig. 1.

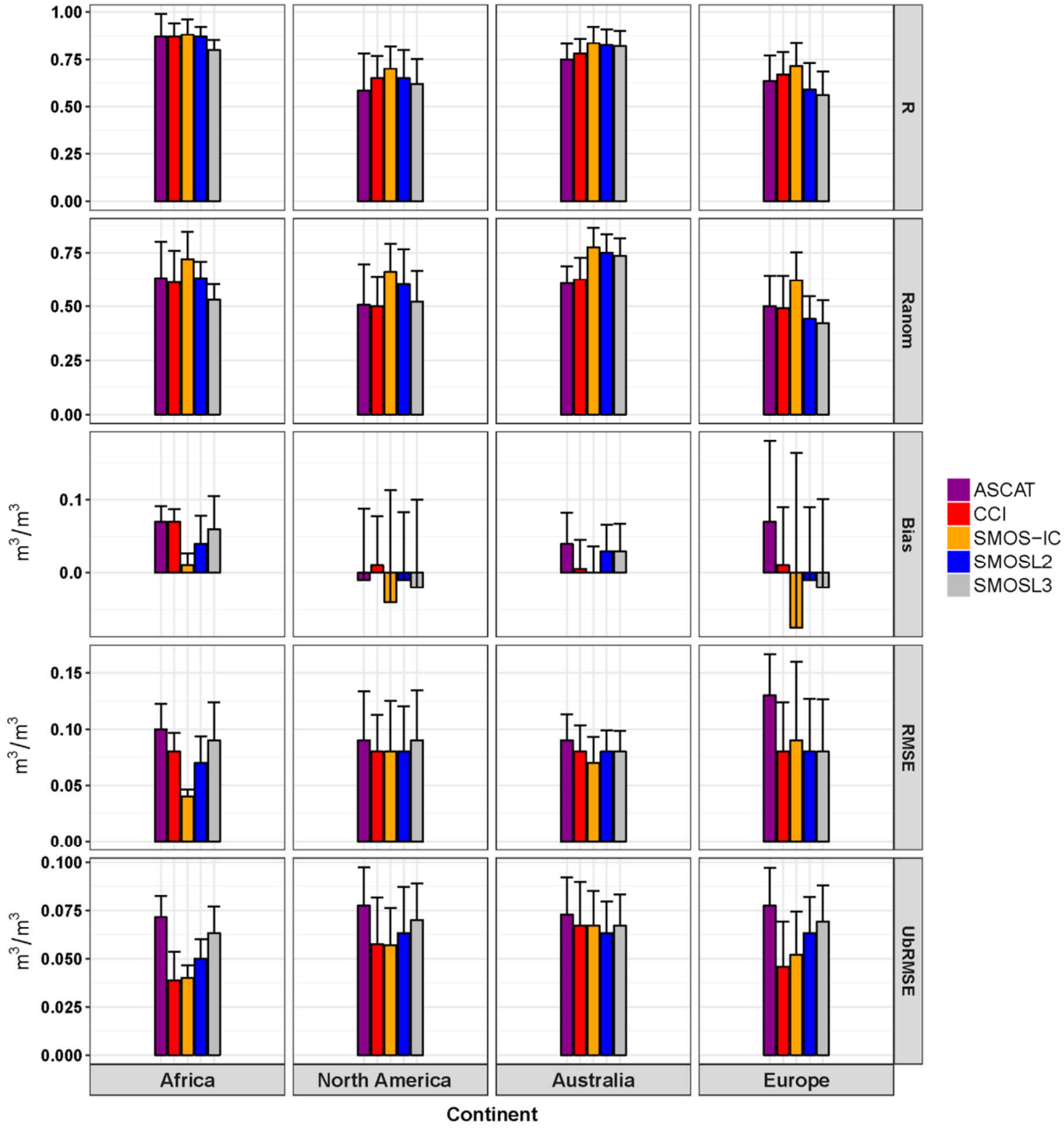

Figure 3 Same as Figure 2, but now excluding SMAP and extending the evaluation period to common data points in 2010-2017, over America (n=393 stations), Australia (n=28 stations), Europe (n=94 stations), and Africa (n=13 stations).

3.3 Impact of vegetation and climate

For the ISMN networks used in this study, climate and land cover can be quite heterogeneous in some continents (e.g. America, Europe) and relatively homogeneous in others (e.g. Australia, Africa). So in this section we analyze more in depth the impact of vegetation and climate on the performances of the satellite-based SM products.

3.3.1 Vegetation

There is consensus among the SM community that vegetation density affects the remotely-sensed SM quality (Jackson et al., 1982; Wigneron et al., 2017). Earlier studies (e.g., Al-Yaari et al., 2014a; Al-Yaari et al., 2014b) found that the performance of the satellite-based SM products varies depending on the vegetation density and land cover type. This section is devoted to re-evaluate the impact of vegetation on the performance of SM products using new SM versions/products. Given the fact that all SMOS products (i.e. SMOS-IC, SMOSL3, and SMOSL2) use SMOS TB observations and ECMWF soil temperature data, they are not totally independent. Also, there is slightly better performance of SMOS-IC over the other SMOS products. Therefore, to simplify the inter-comparison, this section is limited to the SMOS-IC version and other none-SMOS products. The evaluation scores (for all stations) i.e. R, R_{anom}, Bias, RMSE, and ubRMSE are stratified based on the IGBP land cover type (see Fig. S1 in the supplementary). Results, based only on common dates within the period 2015-2016 (2 years), are displayed in Fig. 4.

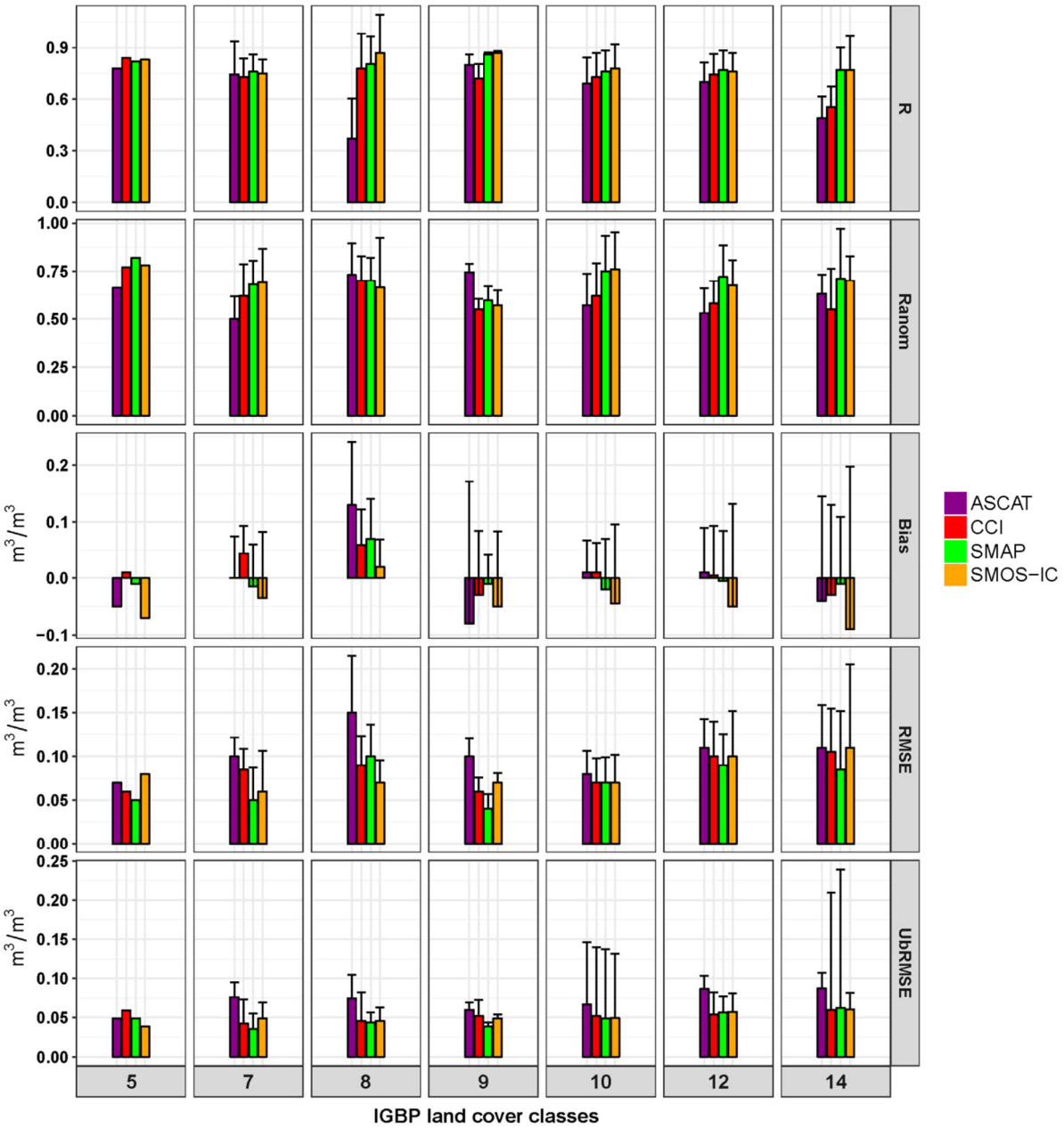

538

539 *Figure 4 Median metrics (R, R_{anom}, Bias, RMSE, and ubRMSE) of all sites stratified by IGBP land*
540 *cover type (see Fig. S1) for SMOS-IC, ASCAT, CCI, and SMAP: Mixed forest (5; n=1 station), Open*
541 *shrublands (7; n=10 stations), Woody savannas (8; n=8 stations), Savannas (9; n=27 stations),*
542 *Grasslands (10; n=132 stations), Croplands (12; n=67 stations) , Cropland/Natural vegetation*
543 *mosaic (14; n=22 stations). n denotes the number of stations per land cover type. Error bars*
544 *represent the standard deviation (SD; variability) of stations (median+SD). Only data points at*
545 *common dates within the period 2015-2017 are included.*

546

547

548

In terms of correlation (R), similar performances between the four products (SMOS-IC, ESA CCI SM, ASCAT, and SMAP) were found over "Open shrublands", "Croplands", and "Mixed forest". A notable difference between ASCAT (lower performance) and the other three products was found over "Woody savannas". SMOS-IC and SMAP had best correlations with the ISMN observations over "Cropland/Natural vegetation mosaic". SMAP and SMOS-IC had the highest anomaly correlations over "Grasslands" and "Croplands". ASCAT was correlating better to *in situ* measurements anomalies over "Savannas". All the four products agree in terms of sign of the bias value: while all underestimated the ISMN observations over "Cropland/Natural vegetation mosaic" and "Savannas", they all overestimated the ISMN observations over "Woody savannas". However, there is no agreement between products in terms of sign of the bias over all other land cover types. In terms of RMSE and ubRMSE, while ASCAT had generally the highest values, the other three SM products performed similarly over most of the land cover types.

A different insight on the impact of vegetation on the performance of satellite-based SM retrievals with respect to the ISMN *in situ* observations can be seen in Fig. 5. Fig. 5 displays the median of all the statistics considered in this study stratified based on MODIS LAI categories: 0-1, 1-2, and 2-3 m^2/m^2 (see Fig. S1 for the MODIS LAI map). Evidently, because the prior data masking to locations with less than 5 kg/m^2 VWC, only limited data are available for evaluation in densely vegetated areas. It can be noticed from this figure that there is an increase in ubRMSE for all remotely-sensed SM products with increasing vegetation density. For SMAP and ESA CCI there is a high variability of their performances among stations as indicated by the high standard deviation over the LAI 2-3 category. In terms of R, similar performances among products can be noticed over the category 0-1 but better performance was obtained by SMOS-IC going from 0-1 to 2-3 categories, whereas ASCAT retrievals degraded for denser vegetation. The best R_{anom} values were obtained by

SMOS-IC (followed by ASCAT) and SMAP (followed by SMOS-IC) over the 2-3 and 1-2 categories, respectively. SMOS-IC and SMAP performed similarly in terms of R_{anom} over the 0-1 category. In terms of ubRMSE, none is superior over all LAI categories. For instance, while SMAP, SMOS-IC, ESA CCI SM products had similar ubRMSE values over regions with LAI values ranging between 0 and 2 m^2/m^2, SMOS-IC and SMAP had lowest values over the LAI 2-3 category. The four products only agree in terms of sign of bias (dry) over LAI 1-2 category and higher Bias values were obtained by SMOS-IC.

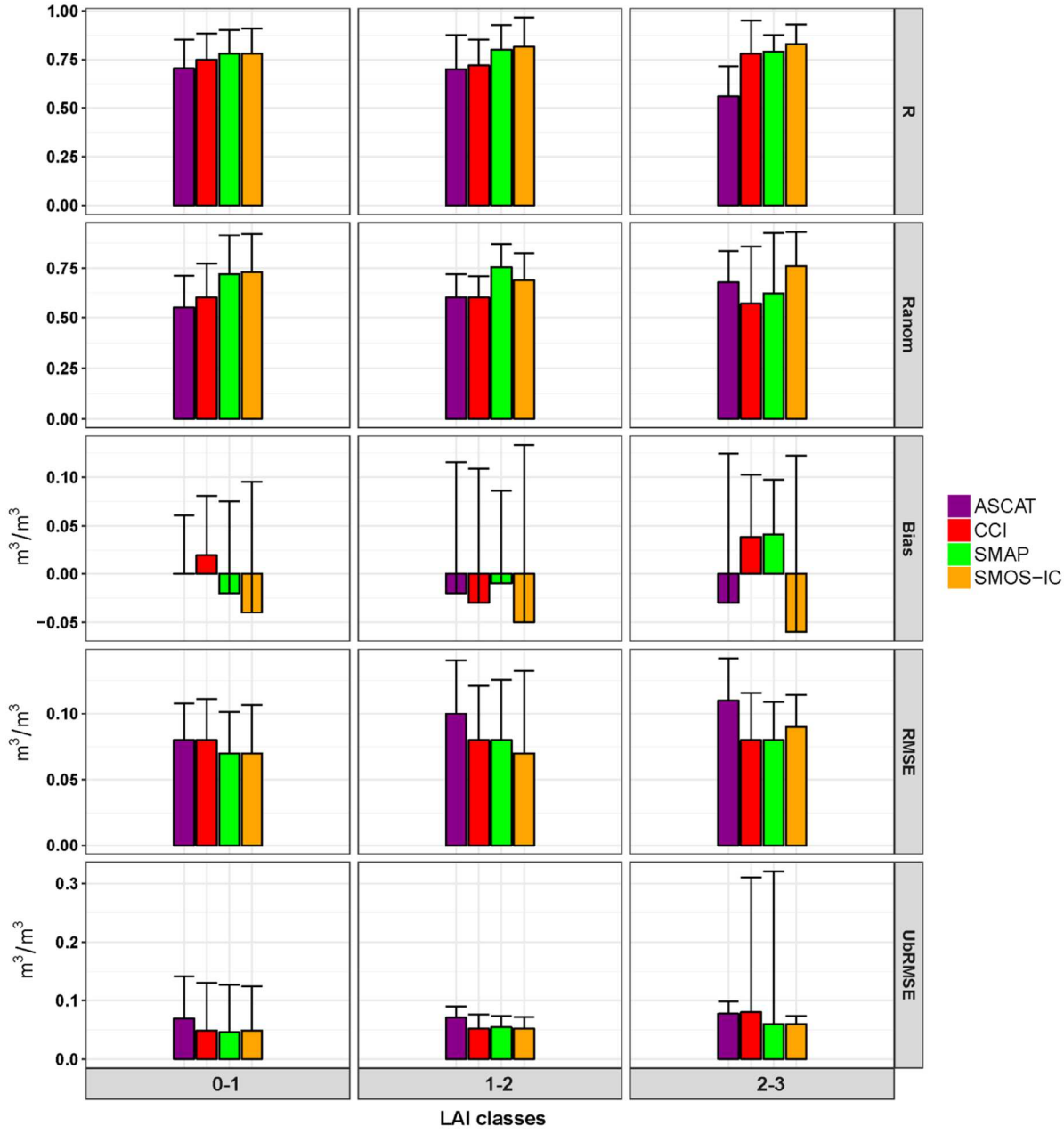

Figure 5 Same as Figure 4, but now grouped by LAI values in 3 classes: 0-1, 1-2, 2-3 m^2/m^2. Number of stations per category: 0-1 (n=160 stations), 1-2 (n=99 stations), 2-3 (n= 9 stations).

3.3.2 Climate

Climate is another factor that can impact the performance of the remotely-sensed SM products. In this study, we assessed the relationship between satellite performance metrics and the Köppen-Geiger climate classification (Kottek et al., 2006). Fig. 6 displays the median of all the statistics considered in this study as a function of Köppen-Geiger main climates (see Fig. S1 for the Köppen-Geiger map): "Equatorial (Savanna) climates: (A)", "Arid and semi-arid climates (B)", "Warm temperate climates (C)", and "Cold climates (D)". It can be noticed from this figure that there is a high variability in the performance of the satellite-based products over regions classified as "B", "C", and "D" in terms of Bias. All remotely-sensed SM products have comparable performances (with small differences) in terms of correlations over "A", "B", and "D" climates in terms of R. The lowest correlations and highest RMSE and ubRMSE values for all products were obtained over "cold climates" climate. SMAP and SMOS-IC correlated better to the ISMN observations over "warm temperate climates" climates than ESA CCI and ASCAT. ASCAT had higher RMSE and ubRMSE over all the main climates and lower R_{anom} over "B", "C", and "D". However, ASCAT had higher correlations (both original and anomalies) over "Equatorial (Savana) climates". The correlations values computed based on anomalies were lower than the original ones particularly over "Equatorial (Savana) climates" and the performance is more spread over the stations. SMAP had a higher R_{anom} over "cold climates" but comparable with SMOS-IC over "Arid and semi-arid climates" and "warm temperate climates" and with SMOS-IC and CCI over "Equatorial (Savana) climates". In terms of anomalies, the rank of the products did not change over "Arid and semi-arid climates". With the exception of CCI, remotely-sensed SM products had underestimated *in situ* observations over "warm temperate climates" and "cold climates" and overestimated the ISMN SM observations over "Equatorial (Savana) climates". With the exception of ASCAT, all products had comparable ubRMSE

values over “B”, “C”, and “D” regions. Moreover, “Arid and semi-arid climates” region exhibits high variability in terms of performance scores.

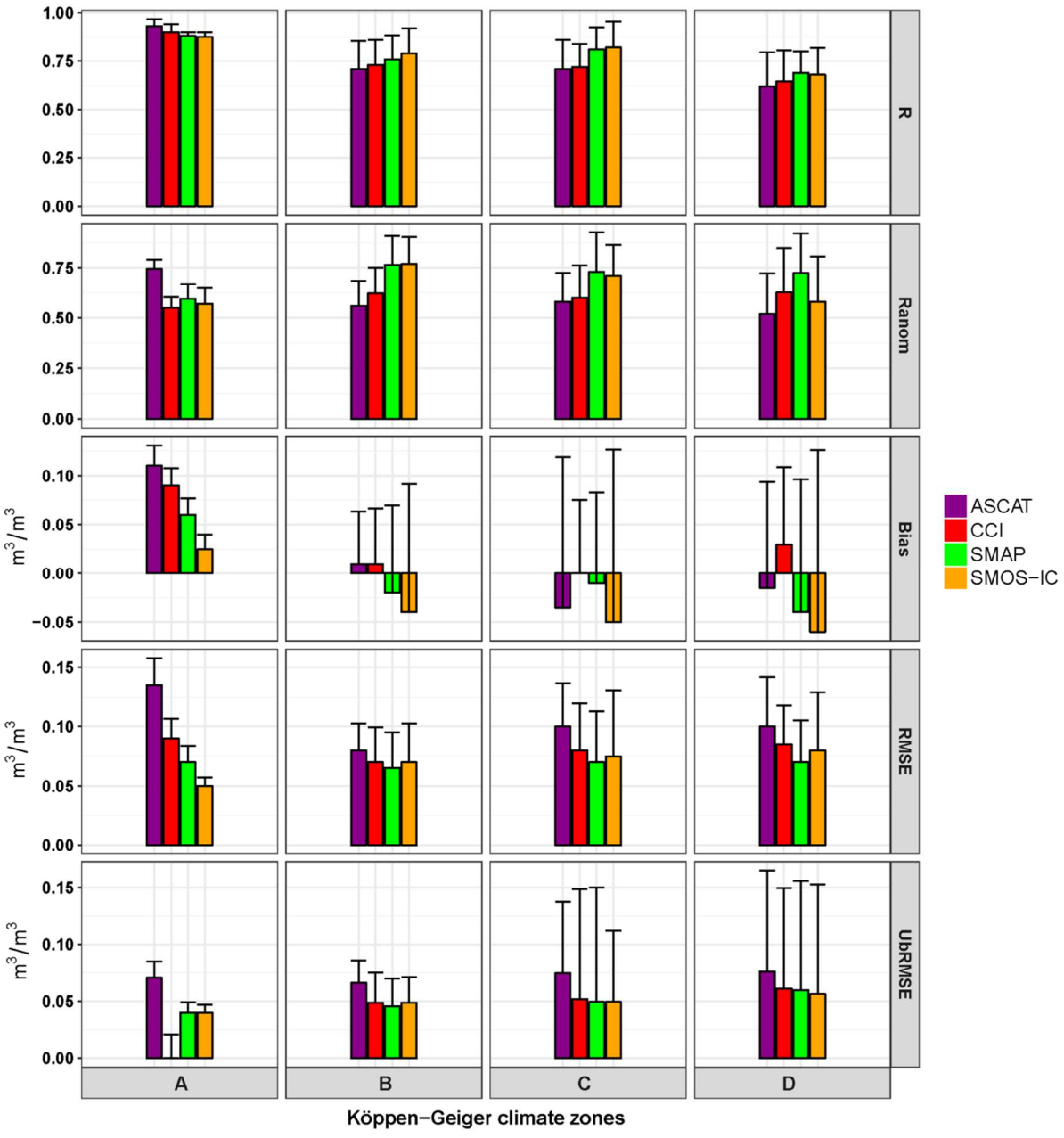

Figure 6 Same as Figure 4, but now grouped by Köppen-Geiger main climates (see Fig. S1). A: Equatorial (Savanna; n= 8 stations), B: Arid and semiarid (n=90 stations), C: Warm temperate climates (n=132 stations), D: Cold climates (n=42 stations). Source of the climate classifications: (Kottek et al., 2006).

4. Discussion

Based on the evaluation results shown above in Figs. 1-3, it was found that comparing remotely-sensed SM product to the ISMN in-situ measurements individually (i.e. taking all available observations) or limiting observations to the availability of the other remotely-sensed SM products can impact the evaluation scores and the ranking of the various SM retrieval products, due to differences in spatial and temporal sampling. On the one hand, considering all observations, SMAP and SMOS-IC gave the best performance in terms of correlations (Fig. 1), while on the other hand, they had similar performance to SMOSL2 and SMOSL3 when considering only common dates over the Australia network (Fig. 2). Another example concerns stations situated over Africa, where ASCAT provided the highest correlation value (though the differences were small) when considering all observations (Fig. 1) but when considering only observations collocated with the other products, a similar performance with CCI, SMOSL2, and SMOS-IC (Fig. 3) was obtained.

In some cases, the performances were unchanged when cross masking data. This may be coincidence, or it may indicate that the masked data are indeed a representative subsample of all data. For instance, in terms of ubRMSE, ESA CCI SM was the best in all cases over Europe. SMOS-IC was the best for ubRMSE and this position was unchanged whether all observations were considered (Fig. 1) or considering only common dates (Figs. 2 and 3) over the Australian network. All remotely-sensed SM products were consistently wetter than the ISMN SM products over the African and Australian networks in all cases considered in this study i.e. using all observations or only common dates. Similarly, the small bias in dryness (wetness) of ASCAT, SMAP, and SMOS (ESA CCI SM) with respect to the ISMN observations over stations located in the U.S. persisted, regardless of the data masking. The dryness of SMAP is in line with previous studies conducted by Chen et al. (2017b), over the Tibetan Plateau. The presence of bias is a common problem of the remotely-sensed SM

products analyzed in this study. Other than the representativeness errors between the point-scale in situ measurements and coarse-resolution space borne products, the absolute value of Bias is affected by (Al Bitar et al., 2017; Draper et al., 2009; Escorihuela et al., 2010; Jackson et al., 2012): different sensing depths (and thus observed volume), the use of auxiliary variables from models (e.g., soil temperature), uncertainties due to the *in situ* sensor errors, scaling and conversion of units (mainly for ESA CCI SM and ASCAT), and spatial heterogeneity.

Overall, the ubRMSE is larger than the target uncertainty of 0.04 m^3/m^3 when doing an evaluation against sparse networks, which suffer largely from representativeness error. It is worth noting that the ubRMSE values (particularly for SMAP) found in this study are in line with those found by El Hajj et al. (2018), but larger than those found by Colliander et al. (2017) and Chan et al. (2016). These later studies used core validation sites, which have significantly smaller representation errors through upscaling of the dense SM networks; here we considered the median value of the scores of individual stations within continents, land cover types, or climate zones. Furthermore, it was shown that ASCAT generally had the highest ubRMSE values compared to other products over most of the networks and lower correlations over arid environments. This could be explained by volume scattering in dry sands and the fact that the ASCAT product is given as a degree of saturation unit, which was converted to the volumetric units (i.e. m^3/m^3) using soil porosity information (Wagner et al., 2013). Soil porosity datasets are often not very accurate (Brocca et al., 2011), and they may significantly affect the Bias and ubRMSE scores obtained by ASCAT. In addition, it should be noted that the Bias values obtained for ESA CCI are imposed by the GLDAS Noah model, as already mentioned above.

The increase in R values when only common data points are used is most likely because less stations are included, which each now has a more complete time series, allowing to sample more of the long-term variability. When excluding SMAP from the analyses (Fig.

3), SMOS-IC generally (followed by SMOSL2 and ESA CCI in most cases) ranked first in terms of correlations (both original SM values and anomalies) for most of the ISMN stations considered in this study. However, the differences in R values are rather very small. The slightly better performance of SMOS-IC is probably due to the improvements introduced into the algorithm (e.g., limiting the use of auxiliary information, new calibration, etc.). However, SMOS-IC showed higher Bias values comparing to other products which is expected as Bias was considered as the least important metric in the SMOS-IC SM algorithm calibration processes (Fernandez-Moran et al., 2017a).

While the best performances of all remotely-sensed SM products in terms of correlation was found over the Australian and African networks (due to common low vegetation density over these networks), the worst and more diverse results were found over the European networks (particularly SMOS). However, in most cases and particularly for stations located over Africa, anomaly correlations were lower than for the original correlations, which means that the correlations of those stations were controlled by the annual cycle (pronounced dry and wet seasons). In the case of Europe, the SMOS observations are affected by RFIs plus snow freezing not always well taken into account (partial coverage, human impacts) that could partially explain the lower performances of SMOSL2 and SMOSL3 over this continent.

As RFIs signals play a key role in the accuracy of the SM products retrieved from the passive microwave systems, we further analyzed the impact of this factor in Fig. 7 for the SMOS sensor, (times series of observations were too short for the SMAP data which are not included in this analysis). More specifically, the time variation in the quality of the SMOS SM product since 2010 was investigated over the four continents: America, Australia, Africa, and Europe. The correlation values shown in Fig. 7 (upper panel) were calculated for each year separately between the SMOS-IC and ISMN data and then only the median of all sites

721 per continent and year was retained. In Fig. 7 (upper panel), it can be seen that the
722 performance of SMOS-IC over America is stable with no substantial differences between
723 years. Over Australia and Europe (except for 2015), there is a small tendency of increasing
724 correlations from 2010 onwards. Over Africa, there is no obvious trend as the performance of
725 SMOS-IC changes from one year to the other. In order to investigate the effect of RFI on the
726 SMOS-IC results in Fig. 7 (upper panel), the temporal mean of the RMSE of the fit between
727 measured and simulated TB (which can be consided as a proxy of RFI impacts on the TB
728 observations) was computed per year and spatially averaged for the same corresponding
729 entire continents; displayed in Fig. 7 (lower panel). While a substantial decrease in RFI can
730 be noticed over America, RFI over Australia keeps stable throught the seven years. Over
731 Africa and Europe, RFI signals effects changed from one year to the other with no general
732 trends. Interestingly, the notable decrease in the performance of SMOS-IC over 2013-2014
733 over Africa and 2015 over Europe correspond to higher RFI levels than in the preceding and
734 following years. So, these figures tend to confirm that the RFI effects may be a key factor to
735 explain time variations in the performance of SMOS-IC over these continents. The lowest
736 RFI signals among continents were found over Australia, which was reflected in the best
737 performance of SMOS-IC in all years in terms of correlations over the continents. The results
738 showed that the performance of SMOS datasets is still highly affected by RFI signals, even if
739 the ESA already put lot of effort in closing down many RFI sources (Oliva et al., 2016). However,
740 this cannot be generalized as for instance over Europe, the TB RMSE decrease in 2011
741 (lower RFI conditions) matches with an R-decrease in SM.

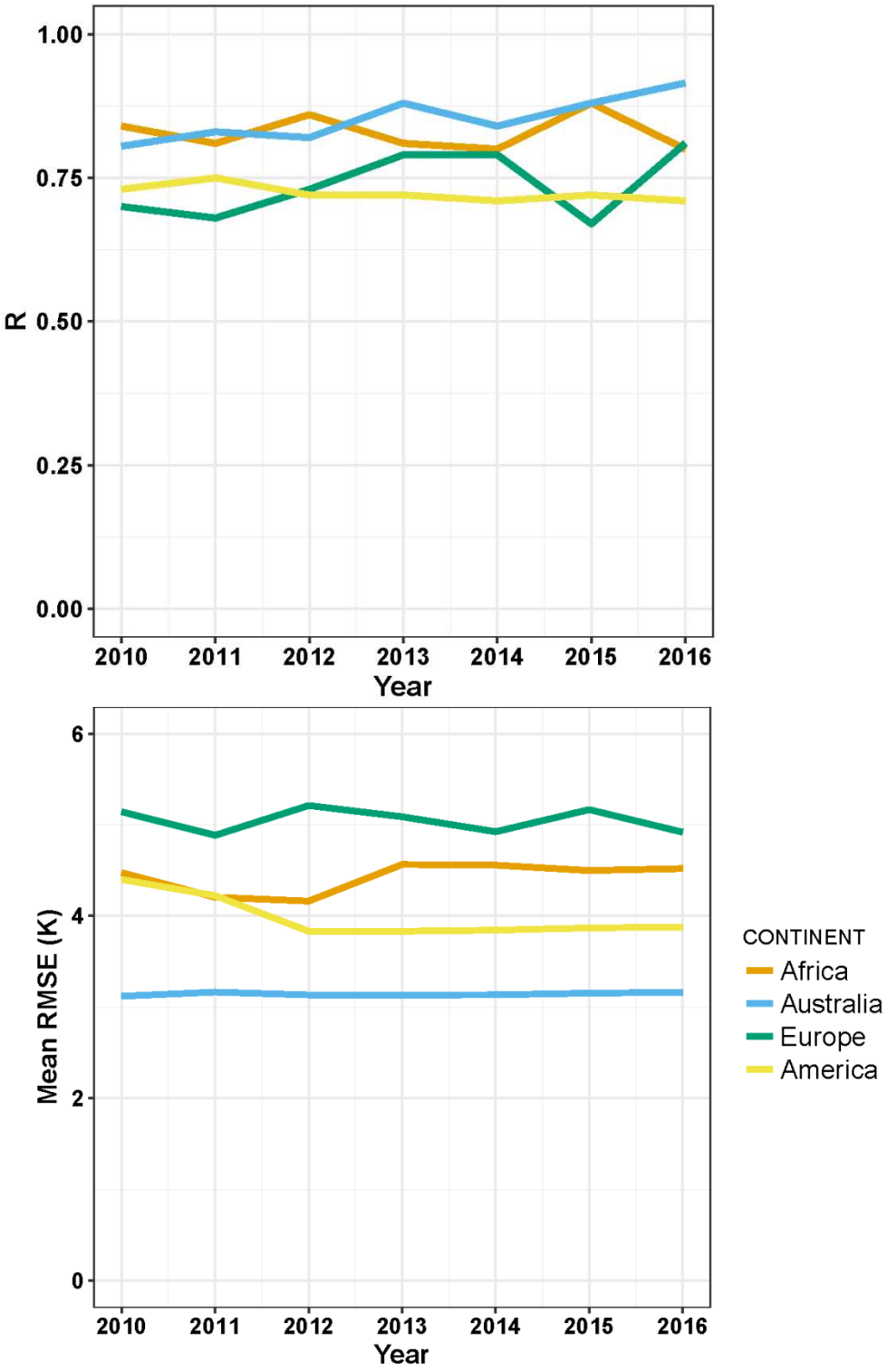

742

743 *Figure 7 Correlation between SMOS-IC SM and the ISMN in situ SM observations (upper panel) and*
744 *RMSE of the fit between measured and simulated TB (bottom panel) during the 2010-2016 period*
745 *over Africa, Europe, America, and Australia. Correlations were calculated per year separately for all*
746 *stations located in the same continent and then the median of all stations was computed.*

747 Other general disturbing factors that impact the performance of the remote sensing
748 SM products over Europe include climate, dense vegetation, or mountains. The regions of
749 SM networks over the African and Australia networks are relatively homogenous with less
750 spatial variability in SM, which led to higher skills of remote sensing retrievals (e.g., Dorigo
751 et al., 2012). In terms of correlations and ubRMSE: while lowest performances (with more
752 variability) of most the remotely-send SM products were obtained for "cold climates", which
753 is expected due to the effects of snow and frozen conditions that are not well filtered or the
754 landscape (vegetation, soil) is very different from the other areas where much of the
755 algorithm development has occurred. Highest performances were obtained over "tropical
756 savanna climates", which is, as mentioned above, mainly controlled by the annual cycle. This
757 indicates that climate and the time series length is a significant factor when comparing
758 satellite-based SM products.

759 The better performance, particularly in terms of temporal dynamics, of SMAP and
760 SMOS-IC over active (ASCAT) products, using only common dates, over regions where LAI
761 range between 2 and 3 m^2/m^2 is probably due to the fact that SMAP and SMOS (and ESA
762 CCI which contains SMOS) operate at L-band which is optimal for SM monitoring: L-band
763 observations have higher penetration capabilities through dense vegetation and lower
764 sensitivity to atmospheric effects such as heavy rainfall events than higher frequencies (C-
765 and X- bands). However, over these regions, ASCAT showed similar R_{anom} as SMAP. Over
766 some land cover types/regions, the ESA CCI SM product was performing similarly to SMOS-
767 IC and SMAP, which is probably due to the fact that it contains SMOS L-band observations.
768 The small difference in correlation values (both R and R_{anom}) between SMOS-IC (higher) and
769 SMAP (lower) over regions where LAI values range between 2 and 3 could be due to the
770 capability of SMOS satellite to measure TB at multi-angular incidence angles and thus better
771 decouple between the soil and vegetation effects. Conversely, the better performance, mainly

772 in terms of ubRMSE of SMAP over the SMOS products is generally due to the improved
773 technology used in SMAP (SMAP has a much better RFI filtering).

774 # 4 Conclusion

775

776 In this study, the assessment and inter-comparison of six recently
777 developed/reprocessed satellite SM products (i.e. SMOS-IC, SMOSL2, SMOSL3, SMAP,
778 ASCAT, and ESA CCI SM) against the ISMN ground-based measurements across different
779 climate and vegetation conditions were conducted. This was accomplished using the Pearson
780 correlation coefficient (R), anomalies (R_{anom}), Bias, RMSE, and ubRMSE metrics. Several
781 conclusions can be drawn from the evaluation presented above:

782 (i) The performance of the six datasets in terms of correlations (temporal dynamics)
783 was rather similar over contrasted biomes and climate conditions, but with a
784 slightly higher skill of both SMAP and SMOS-IC products especially when the
785 data were temporally collocated;

786 (ii) The performances of SM products related to systematic and random errors (i.e.
787 Bias and ubRMSE) varied strongly between products and locations, but with a
788 slightly higher skill of ESA CCI SM, SMOS-IC, and SMAP products. More
789 specifically, similar performances in terms of dryness or wetness with respect to
790 *in situ* observations were obtained over Australia and America, with the exception
791 of ESA CCI SM, regardless of the period or temporal collocation. The six
792 products did not agree in the sign of the Bias over Europe in all of the analyses
793 presented above. Bias strongly depends on the reference data sets and/or model
794 parameters used to determine the absolute SM conditions such as porosity data for
795 ASCAT or GLDAS Noah model for the ESA CCI SM products. Further research

on teasing out and quantifying systematic errors in satellite-based SM retrievals should be recommended for the future;

(iii) When excluding SMAP from the analyses, SMOS-IC was correlating best to the ISMN *in situ* observations and both ESA CCI SM and SMOS-IC presented the lowest ubRMSE values;

(iv) The performance of SMOS-IC, in particular, seems highly impacted by RFI (which is not the case for SMAP or to lesser extent) as indicated by the decrease in correlations values for higher continent-averaged RFI values. RFIs may also to some extent influence the ESA CCI product which integrates both SMOS and AMSR-E/2;

(v) While the best performance (i.e. a better range of correlation values) of all remotely-sensed products was found for stations located in Australia and Africa (semi-arid environments), the worst and more diverse performances were found over Europe (particularly SMOS) and cold climates; and

(vi) A complementarity between ASCAT, SMOS, ESA CCI SM, and SMAP satellite-based SM products was demonstrated in this study given the none superiority of any of them and the different performances of each product over different land cover classes and climate conditions across the globe.

One should be very careful when trying to select the most skillful product, as the performance of each product varies based on the period of evaluation, the evaluation protocol, the data quality control, the number of data points and the study region. These factors could favor one of the products over the others, as it was demonstrated in this study, which makes it a challenge to draw firm conclusions. The SM community is actively working on establishing common guidelines (Gruber et al., in review) for evaluating satellite-based SM

products, which should help future studies in the ranking of various SM products for various applications.

Acknowledgements

This work was jointly supported by CNES (Centre National d'Etudes Spatiales) through the TOSCA (Terre Océan Surfaces Continentales et Atmosphère) program and the European Space Agency (ESA).

.

References

Al-Yaari, A., Wigneron, J.P., Ducharne, A., Kerr, Y., de Rosnay, P., de Jeu, R., Govind, A., Al Bitar, A., Albergel, C., Muñoz-Sabater, J., Richaume, P. & Mialon, A. (2014a). Global-scale evaluation of two satellite-based passive microwave soil moisture datasets (SMOS and AMSR-E) with respect to Land Data Assimilation System estimates. *Remote Sensing of Environment, 149*, 181-195

Al-Yaari, A., Wigneron, J.P., Ducharne, A., Kerr, Y.H., Wagner, W., De Lannoy, G., Reichle, R., Al Bitar, A., Dorigo, W., Richaume, P. & Mialon, A. (2014b). Global-scale comparison of passive (SMOS) and active (ASCAT) satellite based microwave soil moisture retrievals with soil moisture simulations (MERRA-Land). *Remote Sensing of Environment, 152*, 614-626

Al-Yaari, A., Wigneorn, J.P., Ducharne, A., Kerr, Y., Fernandez-Moran, R., Parrens, M., Bi-tar, A.A., Mialon, A. & Richaume, P. (2015). Evaluation of the most recent reprocessed SMOS soil moisture products: Comparison between SMOS level 3 V246 and V272. In, *2015 IEEE International Geoscience and Remote Sensing Symposium (IGARSS)* (pp. 2493-2496)

Al-Yaari, A., Wigneron, J.P., Kerr, Y., Rodriguez-Fernandez, N., O'Neill, P.E., Jackson, T.J., De Lannoy, G.J.M., Al Bitar, A., Mialon, A., Richaume, P., Walker, J.P., Mahmoodi, A. & Yueh, S. (2017). Evaluating soil moisture retrievals from ESA's SMOS and NASA's SMAP brightness temperature datasets. *Remote Sensing of Environment, 193*, 257-273

Al Bitar, A., Mialon, A., Kerr, Y.H., Cabot, F., Richaume, P., Jacquette, E., Quesney, A., Mahmoodi, A., Tarot, S., Parrens, M., Al-Yaari, A., Pellarin, T., Rodriguez-Fernandez, N. & Wigneron, J.P. (2017). The global SMOS Level 3 daily soil moisture and brightness temperature maps. *Earth Syst. Sci. Data, 9*, 293-315

Albergel, C., Rüdiger, C., Carrer, D., Calvet, J.-C., Fritz, N., Naeimi, V., Bartalis, Z. & Hasenauer, S. (2009). An evaluation of ASCAT surface soil moisture products with in-situ observations in Southwestern France. *Hydrology and Earth System Sciences, 13*

Albergel, C., de Rosnay, P., Gruhier, C., Munoz-Sabater, J., Hasenauer, S., Isaksen, L., Kerr, Y. & Wagner, W. (2012). Evaluation of remotely sensed and modelled soil moisture products using global ground-based in situ observations. *Remote Sensing of Environment, 118*, 215-226

Bircher, S., Balling, J.E., Skou, N. & Kerr, Y.H. (2012). Validation of SMOS Brightness Temperatures During the HOBE Airborne Campaign, Western Denmark. *IEEE Transactions on Geoscience and Remote Sensing, 50*, 1468-1482

Brocca, L., Hasenauer, S., Lacava, T., Melone, F., Moramarco, T., Wagner, W., Dorigo, W., Matgen, P., Martínez-Fernández, J., Llorens, P., Latron, J., Martin, C. & Bittelli, M. (2011). Soil moisture

861 estimation through ASCAT and AMSR-E sensors: An intercomparison and validation study
862 across Europe. *Remote Sensing of Environment, 115*, 3390-3408
863 Chan, S., Rajat Bindlish, Peggy O'Neill, Eni Njoku, Tom Jackson, Andreas Colliander, Fan Chen, Mariko
864 Burgin, Scott Dunbar, Jeffrey Piepmeier, Simon Yueh, Dara Entekhabi, Michael H. Cosh, Todd
865 Caldwell, Jeffrey Walker, Xiaoling Wu, Aaron Berg, Tracy Rowlandson, Anna Pacheco,
866 Heather McNairn, Marc Thibeault, José Martínez-Fernández, Ángel González-Zamora, Mark
867 Seyfried, David Bosch, Patrick Starks, David Goodrich, John Prueger, Michael Palecki, Eric E.
868 Small, Marek Zreda, Jean-Christophe Calvet, Wade T. Crow & Kerr, Y. (2016). Assessment of
869 the SMAP Passive Soil Moisture Product. *IEEE Transactions on Geoscience and Remote*
870 *Sensing, 54*, 4994 - 5007
871 Chen, F., Crow, W.T., Colliander, A., Cosh, M.H., Jackson, T.J., Bindlish, R., Reichle, R.H., Chan, S.K.,
872 Bosch, D.D., Starks, P.J., Goodrich, D.C. & Seyfried, M.S. (2017a). Application of Triple
873 Collocation in Ground-Based Validation of Soil Moisture Active/Passive (SMAP) Level 2 Data
874 Products. *IEEE Journal of Selected Topics in Applied Earth Observations and Remote Sensing,*
875 *10*, 489-502
876 Chen, T., McVicar, R.T., Wang, G., Chen, X., de Jeu, A.R., Liu, Y.Y., Shen, H., Zhang, F. & Dolman, J.A.
877 (2016). Advantages of Using Microwave Satellite Soil Moisture over Gridded Precipitation
878 Products and Land Surface Model Output in Assessing Regional Vegetation Water Availability
879 and Growth Dynamics for a Lateral Inflow Receiving Landscape. *Remote Sensing, 8*
880 Chen, Y., Yang, K., Qin, J., Cui, Q., Lu, H., La, Z., Han, M. & Tang, W. (2017b). Evaluation of SMAP,
881 SMOS, and AMSR2 soil moisture retrievals against observations from two networks on the
882 Tibetan Plateau. *Journal of Geophysical Research: Atmospheres, 122*, 5780-5792
883 Colliander, A., Jackson, T.J., Bindlish, R., Chan, S., Das, N., Kim, S.B., Cosh, M.H., Dunbar, R.S., Dang,
884 L., Pashaian, L., Asanuma, J., Aida, K., Berg, A., Rowlandson, T., Bosch, D., Caldwell, T., Caylor,
885 K., Goodrich, D., al Jassar, H., Lopez-Baeza, E., Martínez-Fernández, J., González-Zamora, A.,
886 Livingston, S., McNairn, H., Pacheco, A., Moghaddam, M., Montzka, C., Notarnicola, C.,
887 Niedrist, G., Pellarin, T., Prueger, J., Pulliainen, J., Rautiainen, K., Ramos, J., Seyfried, M.,
888 Starks, P., Su, Z., Zeng, Y., van der Velde, R., Thibeault, M., Dorigo, W., Vreugdenhil, M.,
889 Walker, J.P., Wu, X., Monerris, A., O'Neill, P.E., Entekhabi, D., Njoku, E.G. & Yueh, S. (2017).
890 Validation of SMAP surface soil moisture products with core validation sites. *Remote Sensing*
891 *of Environment, 191*, 215-231
892 Crow, W.T., Berg, A.A., Cosh, M.H., Loew, A., Mohanty, B.P., Panciera, R., Rosnay, P., Ryu, D. &
893 Walker, J.P. (2012). Upscaling sparse ground-based soil moisture observations for the
894 validation of coarse-resolution satellite soil moisture products. *Reviews of Geophysics, 50*
895 Derksen, C., Xu, X., Scott Dunbar, R., Colliander, A., Kim, Y., Kimball, J.S., Black, T.A., Euskirchen, E.,
896 Langlois, A., Loranty, M.M., Marsh, P., Rautiainen, K., Roy, A., Royer, A. & Stephens, J. (2017).
897 Retrieving landscape freeze/thaw state from Soil Moisture Active Passive (SMAP) radar and
898 radiometer measurements. *Remote Sensing of Environment, 194*, 48-62
899 Dorigo, W., de Jeu, R., Chung, D., Parinussa, R., Liu, Y., Wagner, W. & Fernández-Prieto, D. (2012).
900 Evaluating global trends (1988–2010) in harmonized multi-satellite surface soil moisture.
901 *Geophysical Research Letters, 39*, L18405
902 Dorigo, W., Wagner, W., Albergel, C., Albrecht, F., Balsamo, G., Brocca, L., Chung, D., Ertl, M., Forkel,
903 M., Gruber, A., Haas, E., Hamer, P.D., Hirschi, M., Ikonen, J., de Jeu, R., Kidd, R., Lahoz, W.,
904 Liu, Y.Y., Miralles, D., Mistelbauer, T., Nicolai-Shaw, N., Parinussa, R., Pratola, C., Reimer, C.,
905 van der Schalie, R., Seneviratne, S.I., Smolander, T. & Lecomte, P. (2017). ESA CCI Soil
906 Moisture for improved Earth system understanding: State-of-the art and future directions.
907 *Remote Sensing of Environment, 203*, 185-215
908 Dorigo, W.A., Wagner, W., Hohensinn, R., Hahn, S., Paulik, C., Xaver, A., Gruber, A., Drusch, M.,
909 Mecklenburg, S., van Oevelen, P., Robock, A. & Jackson, T. (2011). The International Soil
910 Moisture Network: a data hosting facility for global in situ soil moisture measurements.
911 *Hydrol. Earth Syst. Sci., 15*, 1675-1698

912 Dorigo, W.A., Xaver, A., Vreugdenhil, M., Gruber, A., Hegyiová, A., Sanchis-Dufau, A.D., Zamojski, D.,
913 Cordes, C., Wagner, W. & Drusch, M. (2013). Global Automated Quality Control of In Situ Soil
914 Moisture Data from the International Soil Moisture Network. *Vadose Zone Journal, 12*
915 Dorigo, W.A., Gruber, A., De Jeu, R.A.M., Wagner, W., Stacke, T., Loew, A., Albergel, C., Brocca, L.,
916 Chung, D., Parinussa, R.M. & Kidd, R. (2015). Evaluation of the ESA CCI soil moisture product
917 using ground-based observations. *Remote Sensing of Environment, 162*, 380-395
918 Draper, C.S., Walker, J.P., Steinle, P.J., de Jeu, R.A.M. & Holmes, T.R.H. (2009). An evaluation of
919 AMSR–E derived soil moisture over Australia. *Remote Sensing of Environment, 113*, 703-710
920 Entekhabi, D., Njoku, E.G., O'Neill, P.E., Kellogg, K.H., Crow, W.T., Edelstein, W.N., Entin, J.K.,
921 Goodman, S.D., Jackson, T.J., Johnson, J., Kimball, J., Piepmeier, J.R., Koster, R.D., Martin, N.,
922 McDonald, K.C., Moghaddam, M., Moran, S., Reichle, R., Shi, J.C., Spencer, M.W., Thurman,
923 S.W., Leung, T. & Van Zyl, J. (2010). The Soil Moisture Active Passive (SMAP) Mission.
924 *Proceedings of the IEEE, 98*, 704-716
925 Escorihuela, M.J., Chanzy, A., Wigneron, J.P. & Kerr, Y.H. (2010). Effective soil moisture sampling
926 depth of L-band radiometry: A case study. *Remote Sensing of Environment, 114*, 995-1001
927 Famiglietti, J.S., Ryu, D., Berg, A.A., Rodell, M. & Jackson, T.J. (2008). Field observations of soil
928 moisture variability across scales. *Water Resources Research, 44*
929 FAO, IIASA, ISRIC, ISS-CAS & JRC (2012). Harmonized World Soil Database (version 1.2). FAO and
930 IIASA, Feb 2012. URL http://webarchive. iiasa.ac.at/Research/LUC/External-World-soil-
931 database/HWSD_Documentation.pdf. [Accessed on 20 Nov 2018]
932 Fernandez-Moran, R., Wigneron, J.P., De Lannoy, G., Lopez-Baeza, E., Parrens, M., Mialon, A.,
933 Mahmoodi, A., Al-Yaari, A., Bircher, S., Al Bitar, A., Richaume, P. & Kerr, Y. (2017a). A new
934 calibration of the effective scattering albedo and soil roughness parameters in the SMOS SM
935 retrieval algorithm. *International Journal of Applied Earth Observation and Geoinformation,*
936 *62*, 27-38
937 Fernandez-Moran, R., Al-Yaari, A., Mialon, A., Mahmoodi, A., Al Bitar, A., De Lannoy, G., Rodriguez-
938 Fernandez, N., Lopez-Baeza, E., Kerr, Y. & Wigneron, J.-P. (2017b). SMOS-IC: An Alternative
939 SMOS Soil Moisture and Vegetation Optical Depth Product. *Remote Sensing, 9*
940 Friedl, M.A., Sulla-Menashe, D., Tan, B., Schneider, A., Ramankutty, N., Sibley, A. & Huang, X. (2010).
941 MODIS Collection 5 global land cover: Algorithm refinements and characterization of new
942 datasets. *Remote Sensing of Environment, 114*, 168-182
943 Gruber, A., Dorigo, W.A., Crow, W. & Wagner, W. (2017). Triple Collocation-Based Merging of
944 Satellite Soil Moisture Retrievals. *IEEE Transactions on Geoscience and Remote Sensing, 55*,
945 6780-6792
946 Gruber, A., Clement Albergel., Brian Barrett., Luca Brocca., Andreas Colliander., Michael Cosh, Wade
947 Crow, Richard de Jeu, Wouter Dorigo, Seyed Hamed Alemohammad, Martin Hirschi, A.K.,
948 William Lahoz, Alexander Loew, Kaighin McColl, Nadine Nicolai-Shaw, Robert Parinussa,
949 Chiara Pratola, Sonia Seneviratne, Chun-Hsu Su, Robin van der Schalie, Wolfgang Wagner. &
950 Zwieback, S. (in review). Validation practices for satellite soil moisture products - What are
951 (the) errors? *Remote Sens. Environ*
952 Holgate, C.M., De Jeu, R.A.M., van Dijk, A.I.J.M., Liu, Y.Y., Renzullo, L.J., Vinodkumar, Dharssi, I.,
953 Parinussa, R.M., Van Der Schalie, R., Gevaert, A., Walker, J., McJannet, D., Cleverly, J.,
954 Haverd, V., Trudinger, C.M. & Briggs, P.R. (2016). Comparison of remotely sensed and
955 modelled soil moisture data sets across Australia. *Remote Sensing of Environment, 186*, 479-
956 500
957 Jackson, T.J., Schmugge, T.J. & Wang, J.R. (1982). Passive microwave sensing of soil moisture under
958 vegetation canopies. *Water Resources Research, 18*, 1137-1142
959 Jackson, T.J., Bindlish, R., Cosh, M.H., Tianjie, Z., Starks, P.J., Bosch, D.D., Seyfried, M., Moran, M.S.,
960 Goodrich, D.C., Kerr, Y.H. & Leroux, D. (2012). Validation of Soil Moisture and Ocean Salinity
961 (SMOS) Soil Moisture Over Watershed Networks in the U.S. *Geoscience and Remote Sensing,*
962 *IEEE Transactions on, 50*, 1530-1543

963 Jacquette, E., Al Bitar, A., Cabot, F., Mialon, A., Richaume , P., Quesney, A. & Berthon, L. (2013).
964 CATDS SMOS L3 soil moisture retrieval processor Algorithm Theoretical Baseline Document
965 (ATBD). available at http://www.cesbio.ups-tlse.fr/SMOS_blog/wp-
966 content/uploads/2013/08/ATBD_L3_rev2_draft.pdf . Last access at:01/04/2015
967 Jones, L.A., Kimball, J.S., Reichle, R.H., Madani, N., Glassy, J., Ardizzone, J.V., Colliander, A., Cleverly,
968 J., Desai, A.R., Eamus, D., Euskirchen, E.S., Hutley, L., Macfarlane, C. & Scott, R.L. (2017). The
969 SMAP Level 4 Carbon Product for Monitoring Ecosystem Land–Atmosphere
970 CO₂Exchange. *IEEE Transactions on Geoscience and Remote Sensing, 55*, 6517-
971 6532
972 Jung, M., Reichstein, M., Schwalm, C.R., Huntingford, C., Sitch, S., Ahlström, A., Arneth, A., Camps-
973 Valls, G., Ciais, P., Friedlingstein, P., Gans, F., Ichii, K., Jain, A.K., Kato, E., Papale, D., Poulter,
974 B., Raduly, B., Rödenbeck, C., Tramontana, G., Viovy, N., Wang, Y.-P., Weber, U., Zaehle, S. &
975 Zeng, N. (2017). Compensatory water effects link yearly global land CO2 sink changes to
976 temperature. *Nature, 541*, 516
977 Kerr, Y.H., Waldteufel, P., Wigneron, J.P., Martinuzzi, J., Font, J. & Berger, M. (2001). Soil moisture
978 retrieval from space: the Soil Moisture and Ocean Salinity (SMOS) mission. *IEEE Transactions*
979 *on Geoscience and Remote Sensing, 39*, 1729-1735
980 Kerr, Y.H., Waldteufel, P., Wigneron, J.P., Delwart, S., Cabot, F., Boutin, J., Escorihuela, M.J., Font, J.,
981 Reul, N., Gruhier, C., Juglea, S.E., Drinkwater, M.R., Hahne, A., Martin-Neira, M. &
982 Mecklenburg, S. (2010). The SMOS Mission: New Tool for Monitoring Key Elements ofthe
983 Global Water Cycle. *Proceedings of the IEEE, 98*, 666-687
984 Kerr, Y.H., Waldteufel, P., Richaume, P., Wigneron, J.P., Ferrazzoli, P., Mahmoodi, A., Al Bitar, A.,
985 Cabot, F., Gruhier, C., Juglea, S.E., Leroux, D., Mialon, A. & Delwart, S. (2012). The SMOS Soil
986 Moisture Retrieval Algorithm. *IEEE Transactions on Geoscience and Remote Sensing, 50*,
987 1384-1403
988 Kerr, Y.H., Al-Yaari, A., Rodriguez-Fernandez, N., Parrens, M., Molero, B., Leroux, D., Bircher, S.,
989 Mahmoodi, A., Mialon, A., Richaume, P., Delwart, S., Al Bitar, A., Pellarin, T., Bindlish, R.,
990 Jackson, T.J., Rüdiger, C., Waldteufel, P., Mecklenburg, S. & Wigneron, J.P. (2016). Overview
991 of SMOS performance in terms of global soil moisture monitoring after six years in
992 operation. *Remote Sensing of Environment, 180*, 40-63
993 Kolassa, J., Reichle, R.H., Liu, Q., Alemohammad, S.H., Gentine, P., Aida, K., Asanuma, J., Bircher, S.,
994 Caldwell, T., Colliander, A., Cosh, M., Holifield Collins, C., Jackson, T.J., Martínez-Fernández,
995 J., McNairn, H., Pacheco, A., Thibeault, M. & Walker, J.P. (2018). Estimating surface soil
996 moisture from SMAP observations using a Neural Network technique. *Remote Sensing of*
997 *Environment, 204*, 43-59
998 Koster, R.D., Dirmeyer, P.A., Guo, Z., Bonan, G., Chan, E., Cox, P., Gordon, C.T., Kanae, S., Kowalczyk,
999 E., Lawrence, D., Liu, P., Lu, C.-H., Malyshev, S., McAvaney, B., Mitchell, K., Mocko, D., Oki, T.,
1000 Oleson, K., Pitman, A., Sud, Y.C., Taylor, C.M., Verseghy, D., Vasic, R., Xue, Y. & Yamada, T.
1001 (2004). Regions of Strong Coupling Between Soil Moisture and Precipitation. *Science, 305*,
1002 1138-1140
1003 Kottek, M., Grieser, J., Beck, C., Rudolf, B. & Rubel, F. (2006). World Map of the Köppen-Geiger
1004 climate classification updated. *Meteorologische Zeitschrift, 15*, 259-263
1005 Liu, Y.Y., Dorigo, W.A., Parinussa, R.M., de Jeu, R.A.M., Wagner, W., McCabe, M.F., Evans, J.P. & van
1006 Dijk, A.I.J.M. (2012). Trend-preserving blending of passive and active microwave soil
1007 moisture retrievals. *Remote Sensing of Environment, 123*, 280-297
1008 Masson, V., Champeaux, J.-L., Chauvin, F., Meriguet, C. & Lacaze, R. (2003). A Global Database of
1009 Land Surface Parameters at 1-km Resolution in Meteorological and Climate Models. *Journal*
1010 *of Climate, 16*, 1261-1282
1011 Miralles, D.G., van den Berg, M.J., Gash, J.H., Parinussa, R.M., de Jeu, R.A.M., Beck, H.E., Holmes,
1012 T.R.H., Jiménez, C., Verhoest, N.E.C., Dorigo, W.A., Teuling, A.J. & Johannes Dolman, A.

(2014a). El Niño–La Niña cycle and recent trends in continental evaporation. *Nature Clim. Change, 4*, 122-126

Miralles, D.G., Teuling, A.J., van Heerwaarden, C.C. & Vila-Guerau de Arellano, J. (2014b). Mega-heatwave temperatures due to combined soil desiccation and atmospheric heat accumulation. *Nature Geosci, 7*, 345-349

Mo, T., Choudhury, B.J., Schmugge, T.J., Wang, J.R. & Jackson, T.J. (1982). A model for microwave emission from vegetation-covered fields. *Journal of Geophysical Research: Oceans, 87*, 11229-11237

O' Neill, P., Chan, S., Bindlish, R., Jackson, T., Colliander, A., Dunbar, S., Chen, F., Piepmeier, J., Yueh, S., Entekhabi, D., Cosh, M., Caldwell, T., Walker, J., Wu, X., Berg, A., Rowlandson, T., Pacheco, A., McNairn, H., Thibeault, M., Martínez-Fernández, J., Á, G.-Z., Lopez-Baeza, E., Udall, F., Seyfried, M., Bosch, D., Starks, P., Holifield, C., Prueger, J., Su, Z., Velde, R.v.d., Asanuma, J., Palecki, M., Small, E., Zreda, M., Calvet, J.C., Crow, W. & Kerr, Y. (2017). Assessment of version 4 of the SMAP passive soil moisture standard product. In, *2017 IEEE International Geoscience and Remote Sensing Symposium (IGARSS)* (pp. 3941-3944)

Oliva, R., Daganzo, E., Richaume, P., Kerr, Y., Cabot, F., Soldo, Y., Anterrieu, E., Reul, N., Gutierrez, A., Barbosa, J. & Lopes, G. (2016). Status of Radio Frequency Interference (RFI) in the 1400–1427 MHz passive band based on six years of SMOS mission. *Remote Sensing of Environment, 180*, 64-75

Parrens, M., Zakharova, E., Lafont, S., Calvet, J.C., Kerr, Y., Wagner, W. & Wigneron, J.P. (2012). Comparing soil moisture retrievals from SMOS and ASCAT over France. *Hydrology and Earth System Sciences, 16*, 423-440

Parrens, M., Wigneron, J.-P., Richaume, P., Mialon, A., Al Bitar, A., Fernandez-Moran, R., Al-Yaari, A. & Kerr, Y.H. (2016). Global-scale surface roughness effects at L-band as estimated from SMOS observations. *Remote Sensing of Environment, 181*, 122-136

Paulik, C., Dorigo, W., Wagner, W. & Kidd, R. (2014). Validation of the ASCAT Soil Water Index using in situ data from the International Soil Moisture Network. *International Journal of Applied Earth Observation and Geoinformation, 30*, 1-8

Pierdicca, N., Luca, P., Fabio, F., Raffaele, C. & Marco, T. (2013). Analysis of two years of ASCAT- and SMOS-derived soil moisture estimates over Europe and North Africa. *EUROPEAN JOURNAL OF REMOTE SENSING, 46*, 759-773

Pitman, A.J. (2003). The evolution of, and revolution in, land surface schemes designed for climate models. *International Journal of Climatology 23*, 479–510

PUM (2016). Product User Manual (PUM) Soil Moisture Data Records, Metop ASCAT Soil Moisture Time Series. *Doc. No: SAF/HSAF/CDOP2/PUM, v0.4, 2016. http://hsaf.meteoam.it/documents/PUM/SSM_ASCAT_DR_PUM_v0.4.pdf*

Reichle, R.H., De Lannoy, G.J.M., Liu, Q., Ardizzone, J.V., Colliander, A., Conaty, A., Crow, W., Jackson, T.J., Jones, L.A., Kimball, J.S., Koster, R.D., Mahanama, S.P., Smith, E.B., Berg, A., Bircher, S., Bosch, D., Caldwell, T.G., Cosh, M., González-Zamora, Á., Holifield Collins, C.D., Jensen, K.H., Livingston, S., Lopez-Baeza, E., Martínez-Fernández, J., McNairn, H., Moghaddam, M., Pacheco, A., Pellarin, T., Prueger, J., Rowlandson, T., Seyfried, M., Starks, P., Su, Z., Thibeault, M., van der Velde, R., Walker, J., Wu, X. & Zeng, Y. (2017). Assessment of the SMAP Level-4 Surface and Root-Zone Soil Moisture Product Using In Situ Measurements. *Journal of Hydrometeorology, 18*, 2621-2645

Rodell, M., Houser, P.R., Jambor, U., Gottschalck, J., Mitchell, K., Meng, C.J., Arsenault, K., Cosgrove, B., Radakovich, J., Bosilovich, M., Entin, J.K., Walker, J.P., Lohmann, D. & Toll, D. (2004). The Global Land Data Assimilation System. *Bulletin of the American Meteorological Society, 85*, 381-394

Rodríguez-Fernández, J.N., Kerr, H.Y., van der Schalie, R., Al-Yaari, A., Wigneron, J.-P., de Jeu, R., Richaume, P., Dutra, E., Mialon, A. & Drusch, M. (2016). Long Term Global Surface Soil

1063 Moisture Fields Using an SMOS-Trained Neural Network Applied to AMSR-E Data. *Remote*
1064 *Sensing, 8*
1065 Rubel, F., Brugger, K., Haslinger, K. & Auer, I. (2017). The climate of the European Alps: Shift of very
1066 high resolution Köppen-Geiger climate zones 1800–2100. *Meteorologische Zeitschrift, 26*,
1067 115-125
1068 Sahoo, A.K., Houser, P.R., Ferguson, C., Wood, E.F., Dirmeyer, P.A. & Kafatos, M. (2008). Evaluation
1069 of AMSR-E soil moisture results using the in-situ data over the Little River Experimental
1070 Watershed, Georgia. *Remote Sensing of Environment, 112*, 3142-3152
1071 Saxton, K.E. & Rawls, W.J. (2006). Soil Water Characteristic Estimates by Texture and Organic Matter
1072 for Hydrologic Solutions. *Soil Science Society of America Journal, 70*, 1569-1578
1073 Seneviratne, S.I., Corti, T., Davin, E.L., Hirschi, M., Jaeger, E.B., Lehner, I., Orlowsky, B. & Teuling, A.J.
1074 (2010). Investigating soil moisture–climate interactions in a changing climate: A review.
1075 *Earth-Science Reviews, 99*, 125-161
1076 Seneviratne, S.I., Wilhelm, M., Stanelle, T., van den Hurk, B., Hagemann, S., Berg, A., Cheruy, F.,
1077 Higgins, M.E., Meier, A., Brovkin, V., Claussen, M., Ducharne, A., Dufresne, J.-L., Findell, K.L.,
1078 Ghattas, J., Lawrence, D.M., Malyshev, S., Rummukainen, M. & Smith, B. (2013). Impact of
1079 soil moisture-climate feedbacks on CMIP5 projections: First results from the GLACE-CMIP5
1080 experiment. *Geophysical Research Letters, 40*, 5212-5217
1081 Su, C.-H., Ryu, D., Young, R.I., Western, A.W. & Wagner, W. (2013). Inter-comparison of microwave
1082 satellite soil moisture retrievals over the Murrumbidgee Basin, southeast Australia. *Remote*
1083 *Sensing of Environment, 134*, 1-11
1084 Wagner, W., Lemoine, G. & Rott, H. (1999). A Method for Estimating Soil Moisture from ERS
1085 Scatterometer and Soil Data. *Remote Sensing of Environment, 70*, 191-207
1086 Wagner, W., Hahn, S., Kidd, R., Melzer, T., Bartalis, Z., Hasenauer, S., Figa-Saldaña, J., de Rosnay, P.,
1087 Jann, A., Schneider, S., Komma, J., Kubu, G., Brugger, K., Aubrecht, C., Züger, J., Gangkofner,
1088 U., Kienberger, S., Brocca, L., Wang, Y., Blöschl, G., Eitzinger, J. & Steinnocher, K. (2013). The
1089 ASCAT Soil Moisture Product: A Review of its Specifications, Validation Results, and Emerging
1090 Applications. *Meteorologische Zeitschrift, 22*, 5-33
1091 Wigneron, J.P., Waldteufel, P., Chanzy, A., Calvet, J.C. & Kerr, Y. (2000). Two-Dimensional Microwave
1092 Interferometer Retrieval Capabilities over Land Surfaces (SMOS Mission). *Remote Sensing of*
1093 *Environment, 73*, 270-282
1094 Wigneron, J.P., Kerr, Y., Waldteufel, P., Saleh, K., Escorihuela, M.J., Richaume, P., Ferrazzoli, P., de
1095 Rosnay, P., Gurney, R., Calvet, J.C., Grant, J.P., Guglielmetti, M., Hornbuckle, B., Mätzler, C.,
1096 Pellarin, T. & Schwank, M. (2007). L-band Microwave Emission of the Biosphere (L-MEB)
1097 Model: Description and calibration against experimental data sets over crop fields. *Remote*
1098 *Sensing of Environment, 107*, 639-655
1099 Wigneron, J.P., Jackson, T.J., O'Neill, P., De Lannoy, G., de Rosnay, P., Walker, J.P., Ferrazzoli, P.,
1100 Mironov, V., Bircher, S., Grant, J.P., Kurum, M., Schwank, M., Munoz-Sabater, J., Das, N.,
1101 Royer, A., Al-Yaari, A., Al Bitar, A., Fernandez-Moran, R., Lawrence, H., Mialon, A., Parrens,
1102 M., Richaume, P., Delwart, S. & Kerr, Y. (2017). Modelling the passive microwave signature
1103 from land surfaces: A review of recent results and application to the L-band SMOS & SMAP
1104 soil moisture retrieval algorithms. *Remote Sensing of Environment, 192*, 238-262
1105
1106